Zoological Journal of the Linnean Society, 2018, **182**, 107–128. With 7 figures.

Quantitative data on bone vascular supply in lissamphibians: comparative and phylogenetic aspects

AURORE CANOVILLE[1*†], MICHEL LAURIN[2] and VIVIAN DE BUFFRÉNIL[2]

[1]*Steinmann Institute for Geology, Mineralogy and Paleontology, Bonn University, Nußallee 8, 53115 Bonn, Germany*
[2]*CR2P, Centre de Recherches sur la Paléobiodiversité et les Paléoenvironnements, CNRS / MNHN / UPMC (Sorbonne Universités), Muséum National d'Histoire Naturelle, Bâtiment de Géologie, Case postale 48, 43 rue Buffon, F-75231 Paris Cedex 05, France*

Received 19 December 2016; revised 21 February 2017; accepted for publication 19 March 2017

So far, studies documenting bone vascularization patterns have been mainly focused on amniotes. Lissamphibians, generally considered to have poorly vascularized to avascular bone cortices because of their low metabolic rates, have been largely overlooked, and no comparative dataset of bone vascularization exists for this group. To document this aspect of bone microstructure in urodeles and anurans, and to investigate the relationships between cortical vascular density, size, phylogeny and metabolic rate, we sampled 71 species (116 stylopodial elements) encompassing the taxonomic, body size and ecological diversity of the lissamphibians. Our results show that, with the exception of the largest taxon *Andrias*, extant urodeles have generally avascular limb bones; conversely, anurans can exhibit vascular density values equivalent to, or even higher than, those recorded in similar-sized lepidosaurs. Statistical analyses reveal that absolute cortical thickness in stylopod diaphyses is positively correlated to bone vascular density in lissamphibians. However, available data fail to clearly decipher the relationship between metabolism and bone vascularization. Finally, the present study underlines the existence of diverse, sometimes contradictory patterns, and highlights the complexity and multiplicity of the factors likely to influence bone vascular density.

ADDITIONAL KEYWORDS: Anura – bone vascularization – cortical thickness – resting metabolic rate – size threshold – Urodela.

INTRODUCTION

The biological significance of bone vascularization has long been recognized; it has served as one of the main criteria for the classification of bone tissues (e.g. Ricqlès, 1976). The occurrence and abundance of vascular canals is considered an important aspect of bone microstructure because of its complex functional significance. It is indeed supposed to be linked to local (e.g. Buffrénil *et al.*, 2016) or general growth rates (e.g. Castanet *et al.*, 1996a) of the skeleton and the organism as a whole. By extension, the density and spatial organization of bone vascularization have been used as proxies for the metabolic rate of amniotes, considering that this parameter is related to growth rate and thus indirectly related to bone vascularization (Montes *et al.*, 2007; Montes, Castanet & Cubo, 2010). Quantitative models have been developed for this purpose, and applied to extinct taxa in order to assess the growth rates of their bones and their thermal physiologies (Cubo *et al.*, 2012; Huttenlocker & Botha-Brink, 2013, 2014; Legendre *et al.*, 2016).

Experimental data are relatively scarce in support of such inferences, which mainly remain based on empirical clues. Histological observations show that vascular density (VD) in bone is actually related to specific body size or to the size of individual skeletal elements (Ricqlès, 1975; Buffrénil, Houssaye & Böhme, 2008); moreover, VD is high during episodes of fast growth (early ontogenetic stages) and decreases or disappears later in ontogeny (e.g. Cubo *et al.*, 2014).

*Corresponding author. E-mail: canoville.aurore08@gmail.com
†Current address: Paleontology, North Carolina Museum of Natural Sciences, 11 W. Jones Street, Raleigh, NC 27601, USA.

In vivo bone labelling clearly shows that both the density and the orientation of vascular canals are correlated with accretion rate (Castanet *et al.*, 1996a, 2000a; Margerie, Cubo & Castanet, 2002; Margerie *et al.*, 2004). Furthermore, the relationship between basal metabolic rate and VD was substantiated, at least in amniotes, by Montes *et al.*'s (2007) experimental study (see also Cubo *et al.*, 2012).

Cortical vascularization partly reflects the inclusion of periosteal blood vessels into the osteoid in the course of cortical accretion (Morgan, 1959; Brookes, 1963; Trias & Fery, 1979). However, the detailed mechanisms controlling this process are poorly understood. According to Buffrénil *et al.* (2008), only specific size and growth rate significantly influence bone vascularization; however, Cubo *et al.* (2014) proposed a more complex causality, involving, besides histo-metabolic aspects, considerations on the internal architecture and geometry of bones (Cubo *et al.*, 2014). The latter study postulates that VD reflects the needs of bone cells to be supplied with nutrients and to evacuate their metabolic wastes. When bone cortices are very thin, a direct diffusion occurs between the periosteum capillaries and osteocyte canaliculi; in thicker cortices, a vascular network is necessary. Quantitative analyses of the relationship between VD and cortical thickness (CT) support this interpretation in diapsids (Cubo *et al.*, 2014). In addition, the existence of size thresholds (specific size, bone size or bone cross-sectional area), determining the presence of intra-cortical vascularization, has been suggested (Buffrénil *et al.*, 2008; Cubo *et al.*, 2014).

Numerous exceptions or inconsistencies regarding these general interpretative schemes exist (cf. Buffrénil *et al.*, 2008). This situation suggests that other factors are likely to influence vascularization patterns, and that the cascade of causes involving growth rate and metabolic rate that was considered hitherto is not a sufficient explanation. It is thus necessary to increase the amount of comparative data to further document the variability that occurs in the density and spatial organization of bone vascular canals. To date, relevant studies on this topic have mainly focused on extant amniotes (Chinsamy & Elzanowski, 2001; Cubo *et al.*, 2008; Legendre, Segalen & Cubo, 2013; Kolb *et al.*, 2015; Legendre *et al.*, 2016). Lissamphibians, generally considered as having poorly vascularized to avascular bone cortices because of their low metabolism as compared to amniotes (e.g. Padian & Stein, 2013), have been largely overlooked. As a consequence, very few comparative studies on bone vascularization have been specifically conducted in lissamphibians, although the variability of this feature in their long bones has previously been mentioned (Foote, 1911, 1916; Enlow & Brown, 1956, 1958; Ricqlès, 1976; Laurin, Canoville & Quilhac, 2009), and numerous illustrations of bone sections (used in skeletochronological or microanatomical studies) show the presence of vascular canals in some species (Foote, 1916; Canoville & Laurin, 2009; Laurin *et al.*, 2009; Laurin, Canoville & Germain, 2011). A notable exception is the work of Castanet *et al.*, (2003). In this qualitative, comparative study, the authors discussed the general differences in long bone vascular patterns between urodeles and anurans. They noted that urodeles have poorly vascularized to avascular bone cortices. Anurans, to the contrary, have much more diverse and sometimes complex bone structures, with some species showing highly vascularized cortices. They, moreover, observed that the variations in VD seem to be related to the specific body size of anurans, and also the skeletal elements considered. Unfortunately, the different vascular patterns described in Castanet *et al.* (2003) have not been illustrated or quantified.

Three aims are assigned to the present work: (1) further document lissamphibian bone vascularization patterns by sampling a large comparative set of anuran and urodele species; (2) investigate qualitatively and quantitatively the relationships between cortical vascular density, size, phylogeny and metabolic rate; (3) compare our results with previous studies that mostly dealt with amniotes.

MATERIAL AND METHODS

Biological sample

Our biological sample consists of 116 stylopodial elements (55 humeri and 61 femora) for a total of 71 lissamphibian species, representing 34 urodele species (21 genera) and 37 anuran species (29 genera; Table 1), according to the most widely accepted current nomenclature; we are aware that the ranks assigned to these taxa are subjective (Laurin, 2008). All but three are extant species. One humerus plus one femur were available for 45 of these nominal species, whereas ten species are represented only by one humerus and 16 by one femur.

The taxa were sampled to encompass the taxonomic, body size and ecological (aquatic, semi-aquatic and terrestrial) diversity of extant lissamphibians (Table 1 and Appendix; Fig. 1). To investigate a possible influence of size on the VD of bone, we sampled different-sized animals, ranging from small species to the world's largest extant lissamphibian taxa, namely the Goliath frog *Conraua goliath* and the Chinese giant salamander *Andrias davidianus* (Amiet, 2004; Liang, Geng & Zhao, 2004).

Most of the bones were sampled from dried skeletons or specimens preserved in ethanol and curated in the anatomical and herpetological collections of the Museum National d'Histoire Naturelle of Paris,

Table 1. Biological sample of lissamphibians used for histological descriptions

Taxa	Species authority		Specimen numbers (when sampled for the present study)/source of information for histological descriptions	
			Humerus	Femur
Caudata				
Marmorerpeton†	Evans *et al.*, 1988	–	Univ. Coll. London, no n°; Buffrénil *et al.*, 2015	_
Salamander A†	_	_	Univ. Coll. London, no n°; Buffrénil *et al.*, 2015	_
Salamandrella keyserlingii	Dybowski, 1870	Siberian Salamander	_	Smirina, 1994 (fig. 2B)
Hynobius kimurae	Dunn, 1923	Hida Salamander	_	Misawa & Matsui, 1999 (fig. 2D)
Onychodactylus fischeri	Boulenger, 1886	Long-tailed Clawed Salamander	Smirina, Serbinova IA & Makarov, 1994 (fig. 1D)	Smirina, Serbinova IA & Makarov, 1994 (fig. 1D)
Cryptobranchus alleganiensis	Daudin, 1803	Hellbender	MNHN. AC. 1976-170	MNHN. AC. 1976-170
Andrias davidianus	Blanchard, 1871	Chinese Giant Salamander	ZFMK 8568 + ZFMK_unnumbered	ZFMK 8568 + ZFMK_unnumbered
Andrias japonicus	Temminck, 1836	Japanese Giant Salamander	MNHN. AC. 1914-224	MNHN. AC. 1914-224
Siren lacertina	Österdam, 1766	Greater Siren	MNHN. AC. 1888-409	_
Ambystoma andersoni	Krebs & Brandon, 1984	Anderson's Salamander	HISTOS [MNHN] 571	HISTOS [MNHN] 572
Ambystoma opacum	Gravenhorst, 1807	Marbled Salamander	MNHN. AC. 1971-112	MNHN. AC. 1971-112
Salamandra salamandra	Linnaeus, 1758	Common Fire Salamander	MNHN. AC. 1939-135	MNHN. AC. 1939-135
Salamandra lanzai	Nascetti *et al.*, 1988	Lanza's Alpine Salamander	L 2003-1	L 2003-1
Salamandra atra	Laurenti, 1768	Golden Salamander	L 2003-1	L 2003-1
Chioglossa lusitanica	Bocage, 1864	Golden-striped Salamander	Lima, Arntzen JW & Ferrand, 2000 (fig. 1D, E, F)	Lima, Arntzen JW & Ferrand, 2000 (fig. 1D, E, F)
Pleurodeles poireti	Gervais, 1836	Edough Ribbed Newt	_	Francillon & Pascal, 1985 (fig. 1, phot. 4)
Pleurodeles waltl	Michahelles, 1830	Sharp-ribbed Salamander	_	HISTOS [MNHN] 573
Lissotriton boscai	Lataste, 1879	Iberian Newt	Caetano & Leclair, 1999 (fig. 3)	_
Lissotriton vulgaris	Linnaeus, 1758	Smooth Newt	Verrell & Francillon, 1986 (fig. 1B–D)	_
Notophthalmus viridescens	Rafinesque, 1820	Eastern Newt	Caetano & Leclair, 1996 (fig. 2A, B)	_
Ichthyosaura alpestris	Laurenti, 1768	Alpine Newt	Miaud, 1992 (fig. 1, phot. 2)	Smirina & Roček, 1976 (fig. 1A, C); Smirina, 1994 (fig. 2C)
Triturus helveticus	Razoumowsky, 1789	Palmate Newt	Miaud, 1992 (figs 1–4)	_
Triturus montandoni	Boulenger, 1880	Carpathian Newt	L 2003-3	L 2003-3

Table 1. *Continued*

Taxa	Species authority		Specimen numbers (when sampled for the present study)/source of information for histological descriptions	
			Humerus	Femur
Triturus marmoratus	Latreille, 1800	Marbled Newt	Caetano, Castanet & Francillon, 1985 (fig. 3D-F)	Francillon-Vieillot, Arntzen & Géraudie, 1990a (fig. 1A, F; fig. 2C, E)
Triturus cristatus	Laurenti, 1768	Northern Crested Newt	Francillon, 1979 (figs 3, 4)	Francillon-Vieillot, Arntzen & Géraudie, 1990a (fig. 1A, F; fig. 2C, E)
Necturus maculosus	Rafinesque, 1818	Neuse River Waterdog	ZFMK 27706	ZFMK 27706
Proteus anguinus	Laurenti, 1768	Olm	MNHN. AC. 1888-414	MNHN. AC. 1888-414
Amphiuma means	Garden, 1821	Two-toed Amphiuma	MNHN. AC. 1932-184	MNHN. AC. 1932-184
Batrachoseps attenuatus	Eschscholtz, 1833	California Slender Salamander	Wake & Castanet, 1995 (fig. 1D, C)	_
Plethodon glutinosus	Green, 1818	Slimy Salamander	_	MNHN. AC. 1971-106
Plethodon metcalfi	Brimley, 1912	Southern Gray-cheeked Salamander	_	Ash *et al.*, 2003 (fig. 1A, B)
Desmognathus ochrophaeus	Cope, 1859	Allegheny Mountain Dusky Salamander	_	Houck & Francillon, 1988 (fig.1A); Castanet, Francillon-Vieillot & Bruce, 1996b (fig. 5C)
Desmognathus monticola	Dunn, 1916	Seal Salamander	_	Castanet, Francillon-Vieillot & Bruce, 1996b (fig. 3C, D)
Desmognathus quadramaculatus	Holbrook, 1840	Blackbelly Salamander	_	Castanet, Francillon-Vieillot & Bruce, 1996b (fig. 1C, D)
Anura				
Rhinella marina	Linnaeus, 1758	Cane Toad	MNHN. AC. 1885-37	MNHN. AC. 1885-37
Duttaphrynus melanostictus	Schneider, 1799	Black-spectacled Toad	MNHN. H. 149-93	MNHN. H. 149-93
Amietophrynus superciliaris	Boulenger, 1888	African Giant Toad	ZFMK 90569	_
Amietophrynus regularis	Reuss, 1833	African Common Toad	MNHN. H. 163-63.	MNHN. H. 163-63.
Nimbaphrynoides occidentalis	Angel, 1943	Mount Nimba Viviparous Toad	_	Castanet *et al.*, 2000b (fig. 1F)
Epidalea calamita	Laurenti, 1768	Natterjack Toad	HISTOS [MNHN] 2007 to 2011	HISTOS [MNHN] 2007 to 2011
Bufo bufo	Linnaeus, 1758	Common Toad	_	HISTOS [MNHN] 76
Sclerophrys pentoni	Anderson, 1893	Penton's Toad	L 2003-21	Francillon *et al.*, 1984 (figs 3–7)
Atelopus spumarius	Cope, 1871	Pebas Stubfoot Toad	MNHN. H. 2771-6.	MNHN. H. 2771-6.
Hypsiboas boans	Linnaeus, 1758	Rusty Treefrog	L 2003-8	L 2003-8

Table 1. *Continued*

Taxa	Species authority		Specimen numbers (when sampled for the present study)/source of information for histological descriptions	
			Humerus	Femur
Pseudacris triseriata	Wied-Neuwied, 1838	Western Chorus Frog	_	Platz & Lathrop, 1993 (fig. 1)
Agalychnis dacnicolor	Cope, 1864	Mexican Giant Tree Frog	L 2003-10	L 2003-10
Leptodactylus pentadactylus	Laurenti, 1768	South American Bullfrog	L 2003-9	L 2003-9
Ceratophrys aurita	Raddi, 1823	Brazilian Horned Frog	L 2003-5	L 2003-5
Telmatobius culeus	Garman, 1875	Titicaca Water Frog	L 2003-19	L 2003-19
Trichobatrachus robustus	Boulenger, 1900	Hairy Frog	ZFMK 83751	ZFMK 83751
Conraua goliath	Boulenger, 1906	Goliath Frog	ZFMK 15885	ZFMK 15885
Hoplobatrachus occipitalis	Günther, 1858	African Groove-crowned Frog	MNHN. H. 1337.133	MNHN. H. 1337-133
Nanorana vicina	Stoliczka, 1872	Himalaya Paa Frog	MNHN. AC. 1985-1054	MNHN. AC. 1985-1054
Chiromantis rufescens	Günther, 1869	African Foam-nest Treefrog	L 2003-6	L 2003-6
Lithobates catesbeianus	Shaw, 1802	American Bullfrog	MNHN. AC. 1910-367 + L 2003-20	MNHN. AC. 1910-367 + L 2003-20
Lithobates vaillanti	Brocchi, 1877	Vaillant's Frog	L 2003-16	L 2003-16
Lithobates forreri	Boulenger, 1883	Forrer's Grass Frog	L 2003-17	L 2003-17
Rana dalmatina	Bonaparte, 1840	Agile Frog	L 2003-12	L 2003-12
Pelophylax saharicus	Boulenger, 1913	Sahara Frog	Pers. Coll. J. Ben Hassine	Pers. Coll. J. Ben Hassine
Pelophylax ridibundus	Pallas, 1771	Eurasian Marsh Frog	L 2003-14	L 2003-14
Pelophylax esculentus	Linnaeus, 1758	Common Water Frog	L 2003-18	L 2003-18
Rana iberica	Boulenger, 1879	Iberian Frog	L 2003-15	L 2003-15
Rana temporaria	Linnaeus, 1758	European Common Frog	_	MNHN. AC. 1976-165
Pelobates fuscus	Laurenti, 1768	Common Spadefoot	L 2003-11	L 2003-11
Pipa pipa	Linnaeus, 1758	Surinam Toad	MNHN. AC. 1954. 325	MNHN. AC. 1954-325
Pipa carvalhoi	Miranda-Ribeiro, 1937	Carvalho's Surinam Toad	_	MNHN. AC. 1954-325
Xenopus laevis	Daudin, 1802	African Clawed Frog	MNHN. AC. 1939-12	MNHN. AC. 1939-12
Latonia gigantea †	Lartet, 1851	_	_	MNHN/PAL Sa 23480 A, B
Discoglossus pictus	Otth, 1837	Painted Frog	Pers. Coll. J. Ben Hassine	Pers. Coll. J. Ben Hassine
Bombina orientalis	Boulenger, 1890	Oriental Fire-bellied Toad	L 2003-4	L 2003-4
Ascaphus truei	Stejneger, 1899	Coastal Tailed Frog	MNHN. AC. 1968.140	MNHN. AC. 1968-140

Institutional abbreviations: HISTOS [MNHN], Collection d'histologie et de paléohistologie osseuse, Museum National d'Histoire Naturelle, Paris, France; MNHN. AC., Museum National d'Histoire Naturelle, collections d'anatomie comparée, Paris, France; ZFMK, Zoologische Forschungsmuseum Alexander Koenig, Bonn, Germany.
† = Extinct taxa. Note that Salamander A, first mentioned by Evans & Milner (1991), constitutes an unnamed Caudata from the Middle Jurassic. As *Marmorerpeton*, it is probably part of the karaurids, the oldest known stem-urodeles (Evans & Waldman, 1996).

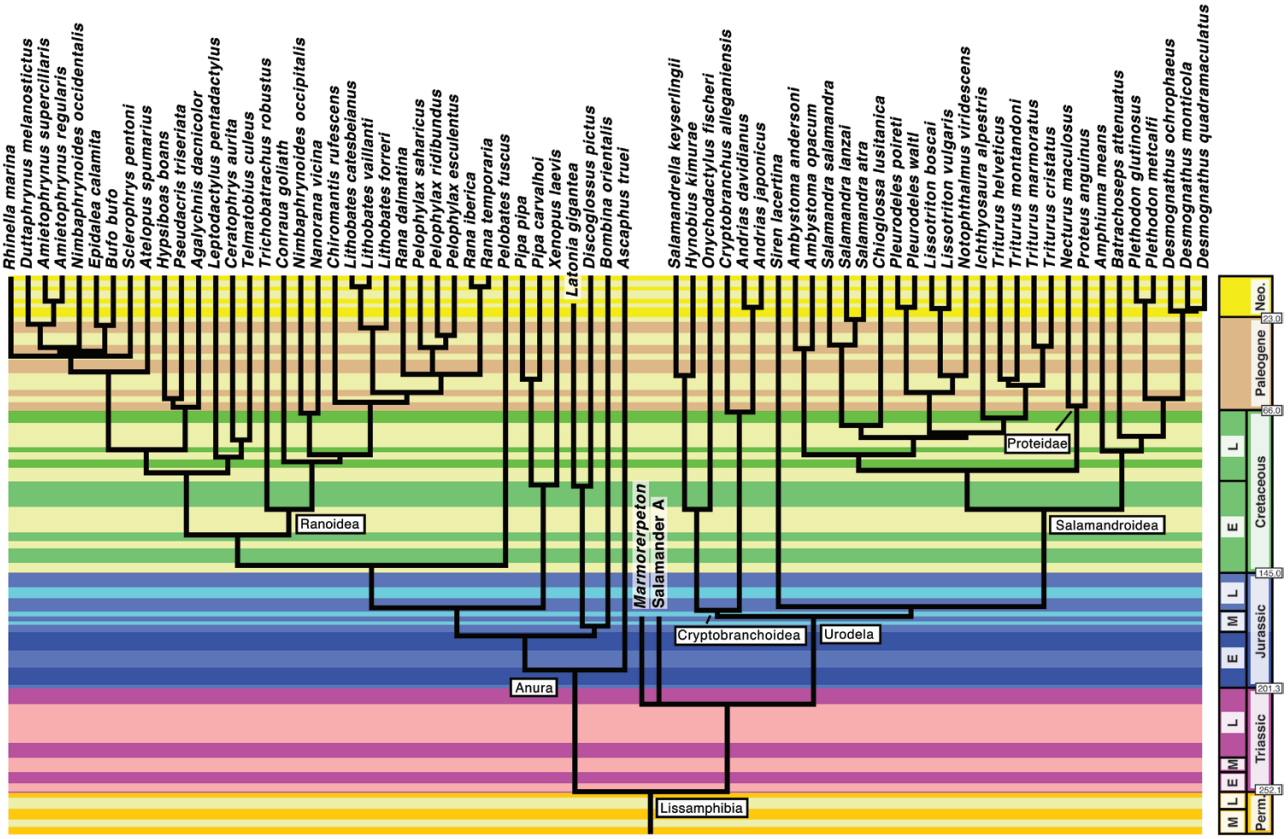

Figure 1. Time calibrated phylogeny of the lissamphibian species sampled in this study. This reference tree was compiled from previously published phylogenies using the Stratigraphic Tools for MESQUITE (Josse, Moreau & Laurin, 2006), and was used for the phylogeny-informed statistical analyses. Abbreviations: E, Early; L, Late; M, Middle; Neo., Neogene; Perm., Permian.

France, and the Zoologische Forschungsmuseum Alexander Koenig, Bonn, Germany (Table 1). All the specimens sampled had a body size superior or equal to 75% of the average adult size known for their species. Our biological sample thus contains mostly adults or sub-adults close to the end of their stage of active somatic growth.

For 20 taxa (Table 1), we used illustrations of complete cross-sections from the literature, if they met the following five criteria: (1) the picture is sharp and precise; (2) the species was clearly identified; (3) the individual was undoubtedly an adult; (4) the cross-section comes from the midshaft of a femur or a humerus; (5) the illustrated bone tissue is avascular. Indeed, in order to standardize our observations, vascular canals were counted only on thin sections studied under the microscope. All taxa with vascularized bones mentioned in the literature were actually represented by specimens in our sample.

In most cases, one specimen per species was sampled. When several specimens were collected for the same species, we used the species means for statistical analyses. Moreover, for each species we recorded, when possible, the presacral length (PLg, in cm). PLg was measured from anterior surface of atlantal centrum to anterior surface of first sacral centrum in urodele skeletons. For fresh specimens, this could not be measured, so we measured from the posterior end of the head to the vent. For anurans, given their very short, stocky body, we measured from the atlantal centrum or caudal end of the head to the posterior end of the urostyle. We also collected data from the literature on the average body mass of each species (BM, in g), as well as the mass-specific resting metabolic rate (ml O_2 g^{-1} h^{-1}) at 15 °C and 20 °C (Appendix).

PROCESSING OF BONE SECTIONS

After manual cleaning (removal of muscle, tendon and medullary tissue residues), the bones were defatted in sequential ethanol and acetone baths, photographed and included in an epoxy resin (Araldite 2020, Huntsman). Two sections of 2 to 10 mm, depending on the size of the bone, were sampled symmetrically from

both sides of a transversal plan to the mid-diaphysis. One of these samples was used for making 2 to 4 transversal thin-sections 80 to 100 µm thick, following standard petrographic procedures (Lamm, 2013). The other block was used for longitudinal thin-sections of the same thickness.

Histological observations, histomorphometric measurements and quantitative parameters

The thin-sections were observed and photographed using an optical microscope (Zeiss Axioskop), under transmitted, normal or polarized light. Vascular canals were identified and counted directly under the microscope. We took into account intra-cortical canals only, and excluded from our observations and counts the large nutrient canals through which the nutrient artery penetrates into bone early in the ossification process. Parameter NC (Appendix) is the total number of vascular canals observed on each thin-section. Drawings of each transversal thin-section were realized at different magnifications (ranging from 40× to 60×, depending on the size of the sections), using a *camera lucida* set on a binocular lens (Zeiss Stemi SV6). All bone microstructural details larger than 10 µm were taken into account (no vascular canals smaller than this were observed in our samples). Once scanned, these drawings were analysed in ImageJ (Abramoff, Magalhães & Ram, 2004) in order to extract five simple quantitative parameters: (1) maximal diameter of the section (MD, in mm); (2) total sectional area (A_{tot}, in mm^2); (3) area of the cortex (A_{cx}, in mm^2); (4) relative area of the cortex expressed in percent of A_{tot} ($RA_{cx} = 100\, A_{cx}/A_{tot}$); (5) absolute cortical thickness (CT, in mm) measured along four orthogonal radii of the section.

The vascular density (VD, in number of vascular canals per mm^2) was calculated as follows: $VD = NC/A_{cx}$. The parameter corresponding to the relative area of the whole set of vascular canals, designated as 'vascular density' by Cubo *et al*. (2005), was not used in the present study, because it could have been misleading. Indeed, in lissamphibians, most of the vascular canals are primary osteons that possess variable lumen widths, depending on the amount of lamellar bone centripetally deposited on their walls.

Non-phylogenetic statistical analyses

Simple (non-phylogenetic) linear regressions and statistical tests were performed in Prism (Graphpad Software Inc.), in order to better visualize the data, and examine the strength and shape of the relationships involving size and bone vascularization. Null hypotheses were rejected at a threshold of $P < 0.05$.

Phylogeny-informed statistical analyses

We tested the presence of a phylogenetic signal by comparing the squared length of each character on the time calibrated reference phylogeny (Fig. 1) with the same statistic on a population of 10 000 random trees. These were obtained by randomly reshuffling the terminal taxa on a tree of fixed branch lengths; this ensures an identical distribution of branch lengths in the reference and random trees (Laurin, 2004). This test was performed to determine whether phylogeny-informed tests should be performed on the data, rather than simple, non-phylogenetic statistics.

Given that some characters show a phylogenetic signal (see below), we also checked whether the hypothesis of Brownian motion evolution of our characters on the reference tree was reasonable. These tests were performed in the PDAP module (Midford, Garland & Maddison, 2010) of Mesquite (Maddison & Maddison, 2014).

Similarly, our findings that most characters evolved according to non-Brownian models (see below) led us to check for character correlation using phylogenetic pairwise comparisons (Maddison, 2000), a phylogeny-informed non-parametric, sign test. This test is less powerful than many other commonly used methods, but it is far more robust to violations of character distribution assumptions, given that it assumes only that evolution has been divergent (rather than reticulate, for instance). Thus, any positive results yielded by this method should be reliable (Maddison & Fitzjohn, 2015).

We tested the hypothesis that vascularization appeared more frequently in anurans than in urodeles using a phylogenetic binomial test as proposed by Smith *et al.* (2013). Basically, this test consists of first determining how many appearances of vascularization occurred in each clade (thus, if a small clade of three anuran taxa shares vascularization, this is scored as a single appearance). Second, the phylogenetic diversity (Faith, 1992) sampled in each clade was determined by first pruning taxa with missing data for the character of interest from the tree. This was done in Mesquite (Maddison & Maddison, 2014), using the Stratigraphic Tools (Josse, Moreau & Laurin, 2006). This procedure aimed to determine the probability of the appearance of the character (per lineage and per million years) occuring in either clade. The test then determines the probability of observing a distribution at least as asymmetrical as that actually observed.

We also tested the hypothesis that the VD was ancestrally the same in both clades. To do this, we used the continuous analysis to check for a significant shift in vascular density. The continuous analysis was proposed by Germain & Laurin (2009) to detect heterochronies, but it can be used to check for a shift in value

between two adjacent nodes on a tree for any quantitative character. In addition, we tested the hypothesis that vascularization appeared more frequently in the humerus than in the femur (something suggested by our observations) using a binomial test on the number of appearances of the vascularization on the reference tree, using parsimony optimization. We did a similar test on the density of vascularization, by comparing the ancestral value for lissamphibians for both bones, and determining whether their 78% confidence intervals overlapped; if they do not, the null hypothesis (that VD of both bones is equal) can be rejected at a 0.05 threshold. The justification for the use of 78% confidence intervals in such tests was briefly presented by Meslin *et al*. (2012), but a more detailed explanation may be useful. This practice is justified by the fact that we are comparing two estimated quantities, rather than a known entity with an estimate. If the real underlying value is the same (which is the null hypothesis), the probability that both intervals will not overlap is the square of 1 – confidence interval width. If we had used 95% confidence intervals, the probability of observing no overlap if the null hypothesis were true would have been 0.05 × 0.05 = 0.0025. Thus, the correct confidence interval width to test whether two nodal values are significantly different is 1 – the square root of the desired probability threshold. For a 0.05 probability threshold of Type 1 error, the square root of 0.05 is 0.2236 (rounded off to the 4th decimal), and 1 – 0.2236 = 0.7764. By rounding off the width of the confidence intervals to 0.78%, we are making the test slightly conservative. The fact that neighbouring nodes on a tree influence each other's value when these are estimated with squared-change parsimony and related methods (Maddison, 1991) should make the test even more conservative.

Given that we performed many tests, we corrected for multiple testing using the false discovery rates (FDR) method (Benjamini & Hochberg, 1995).

RESULTS

Histological observations

Caudata

Cross-sections from the humeri and femora show that the stylopod elements of urodeles have a narrow medullary cavity surrounded by a thick and compact cortex (Fig. 2; Appendix). In *Marmorerpeton*, Salamander A, *A. davidianus*, *Andrias japonicus*, *Ambystoma andersoni*, *Necturus maculosus* and possibly also *Pleurodeles waltl*, bone cortex in both the humerus and femur is perforated by vast erosion cavities displaying a typical scalloped contour (evidence for osteoclast activity). These cavities are irregularly distributed within the cortex, at variable distance from the medullary cavity, and their total area can be much larger than that of the medullary cavity (Fig. 2A). Signs of secondary reconstruction very seldom occur on their walls; it was observed only, to a limited extent, in the two *Andrias* species.

The cortices of all long bones in our sample are made of parallel-fibred tissue (Fig. 2A, B). In cross-section, this tissue appears roughly birefringent in polarized light; however, in some species, the birefringence is poorly characterized (e.g. *N. maculosus* and both *Andrias* species; Fig. 2B, C). Conversely, birefringence is more pronounced in longitudinal sections (Fig. 2E). In most individuals, the rotation of the microscope stage reveals in transversal and longitudinal sections a monorefringent band that moves according to the direction of rotation. These observations suggest that the orientation of collagen fibres in the osseous matrix of urodele long bones is basically longitudinal, but that it also includes a significant spiral component. Osteocyte lacunae appear predominantly circular in transversal sections, with some variability in their morphology and orientation (Fig. 2F). In longitudinal section, they are flattened and oriented parallel to the surface of the cortices (Fig. 2E). Canaliculi are poorly developed (Fig. 2E). The orientation of osteocyte lacunae thus confirms the overall polarization of the bone structure. Sharp cyclical growth marks, in the form of annuli or lines of arrested growth (LAGs), are visible on the cross-sections (Fig. 2C, D).

Urodele long bones are generally avascular; only a few vascular canals were observed in the femur of *A. japonicus* (5 canals, at most, in cross-sections) and *A. davidianus* (2 canals). These are simple vascular canals with average diameters of 60 µm (*A. japonicus*) and 95 µm (*A. davidianus*) and longitudinal to slightly oblique orientations (compared to the long axis of the bone).

In several taxa (e.g. *Andrias*, *Necturus,* etc.), the medullary cavity is still partly or totally obstructed by residues of non-resorbed calcified cartilage at the adult stage (Fig. 2G). This feature reflects neoteny (cf. Ricqlès, 1964, 1965), a fairly common phenomenon in urodeles (Duellman & Trueb, 1986). In the *N. maculosus* specimen, this state only concerns the femur (Fig. 2G), because the medullary cavity of the humerus (Fig. 2B) is devoid of calcified cartilage.

Anura

The long bones of all anuran taxa have a typical tubular architecture, with solid walls void of the wide erosion bays observed in the urodeles (small erosion cavities can be nonetheless present in the perimedullary region). In cross-section, the cortices of anuran long bones are more markedly monorefringent than

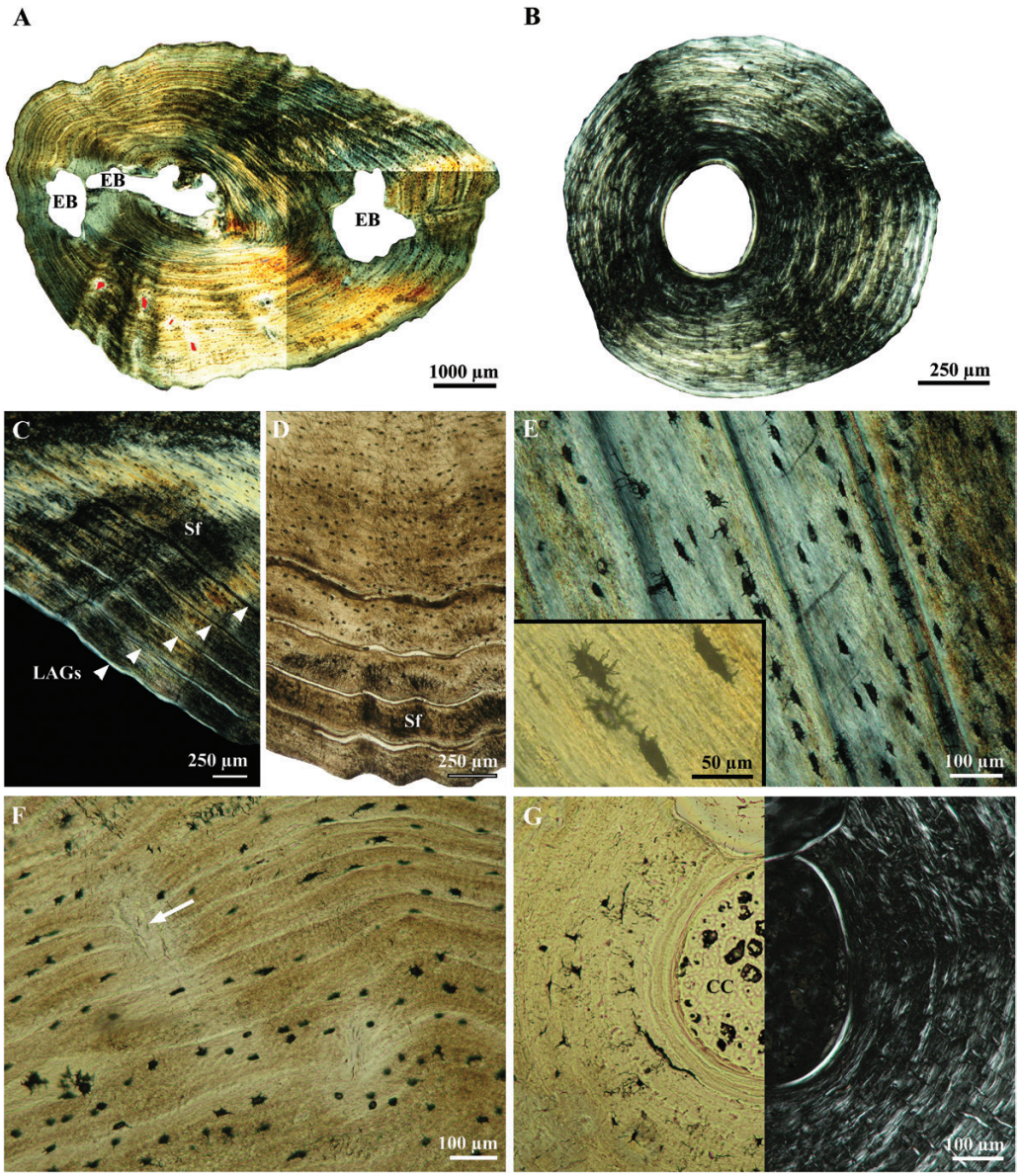

Figure 2. Bone histology of the Caudata. (A) Mid-diaphyseal cross section in *Andrias japonicus* femur (specimen MNHN. AC.1914.224, transmitted polarized light). The bone cortex is globally (but imperfectly) birefringent. The medullary cavity is small, whereas the cortex is very thick, and displays three broad erosion bays, one of which merges into the medullary cavity; (B) Mid-diaphyseal section in *Necturus maculosus* humerus (specimen ZFMK 27706). Same remarks as in the femur of *A. japonicus*; (C–D) Histology of the humeral cortex of *Andrias davidianus* (specimen ZFMK 8568; in polarized and ordinary transmitted light, respectively). Cyclical growth marks, in the form of lines of arrested growth (arrow heads) are particularly pronounced. Note also the abundance in Sharpey's fibres bundles throughout the cortical bone; (E) Longitudinal section in *A. davidianus* femur. The insert is a closer view at osteocyte lacunae; (F) Cross-section in *A. japonicus* femur (ordinary transmitted light). Growth marks are conspicuous throughout the cortex. The white arrow points at one of the rare simple vascular canals observed in the femur of *A. japonicus*; G, calcified cartilage filling the medullary cavity in *N. maculosus* femur. Abbreviations, CC, calcified cartilage; EB, intra-cortical erosion bay; Sf, Sharpey's fibres.

those of the urodeles (Fig. 3A). Likewise, in longitudinal sections, the birefringence of the bone matrix is particularly strong, with alternation of bright and dark phases when rotating the microscope stage (Fig. 3C). These observations indicate that the fibres of the collagenous matrix have a more strictly longitudinal orientation in anurans. In longitudinal sections, osteocyte lacunae appear flat and parallel to the sagittal axis

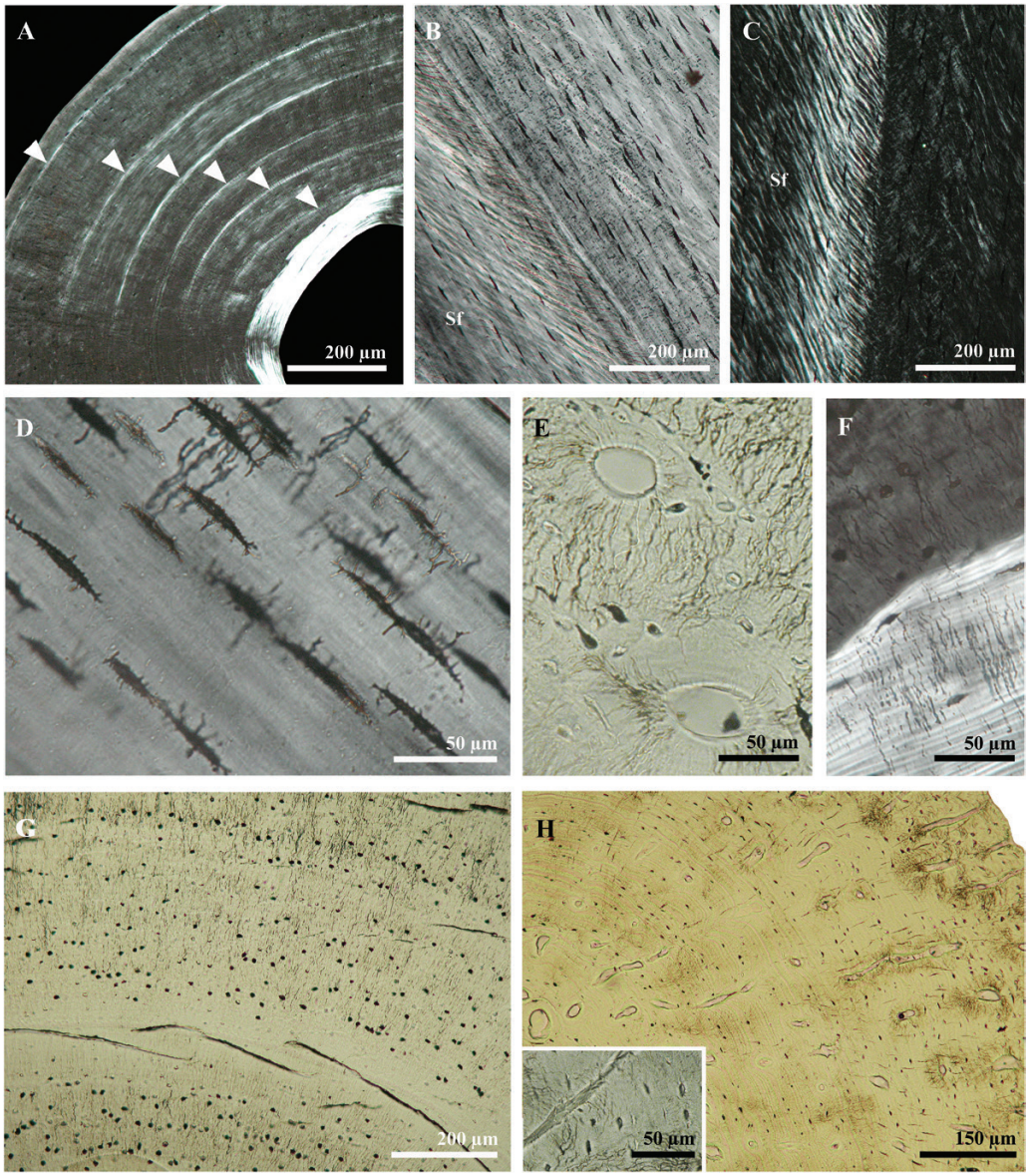

Figure 3. General features of bone histology in the Anura. (A) Cross-section in the femur of *Nanorana vicina* (specimen MNHN AC. 1985-1054; transmitted polarized light). The cortical bone is avascular and isotropic in this sectional plane. Conspicuous birefringent lines of arrested growth occur (arrow heads); (B–C) longitudinal section in the femur of *Conraua goliath* (specimen ZFMK 15885). The bone tissue forming the cortex displays strong birefringence, with total illumination (B) alternating with total extinction (C). Note the presence of numerous bundles of Sharpey's fibres; (D) aspect of osteocyte lacunae in a longitudinal section from the femur of *C. goliath*. The lacunae are oriented parallel to the bone layers, and they display short canaliculi; (E) long, branching canaliculi spreading in the femoral cortex of *Trichobatrachus robustus* (specimen ZFMK 83751); (F) occurrence of such long canaliculi in a thick layer of peri-medullar endosteal bone tissue (in polarized light); (G) rounded aspect of osteocyte lacunae, with long canaliculi, in a cross section of *T. robustus* femur; (H) spindle-like aspect of the osteocyte lacunae in a cross section from *Pipa pipa* humerus (specimen MNHN.AC.1954.325). Insert: closer view at the cell lacunae. Abbreviation: Sf, Sharpey's fibres.

of the bones (Fig. 3D); an aspect confirming that long bone cortices in anurans are made of well-characterized parallel-fibred bone tissue. Sharp cyclical growth marks, in the form of LAGs or birefringent annuli, occur in most anuran bones (Fig. 3A), as also do bundles of radial or oblique Sharpey's fibres (Fig. 3B, C). The main differences between anuran taxa consist of some variability in the regularity of the spatial

orientation of the collagenous meshwork, as well as in the morphology of osteocyte lacunae, which can be circular (Fig. 3G), multipolar or ellipsoid (Fig. 3H) in cross-section.

Although the canaliculi appear short in longitudinal section (Fig. 3D), the cross-sections of most limb bones reveal the presence of complex canalicular networks in the vicinity of the osteocyte bodies (Fig. 3E–H). The aspect of these networks is somewhat reminiscent of the so-called aspidinocytes, which are thin and elongated unmineralized spaces observed in aspidin, a type of acellular bone. The origin and function of these structures have been subject of debates. (Hancox, 1972; see also the critical discussion of this concept in Francillon-Vieillot *et al.*, 1990b). The canaliculi have a primarily radial orientation, but tend to converge towards the lumen of vascular canals, when present (Fig. 3E). It is rare to observe a direct contact between these canalicular extensions and the peri-somatic part of osteocyte lacunae. Their presence in the layer of lamellar endosteal bone (centripetally deposited) surrounding the medullary cavity (Fig. 3F), testifies that these structures are not anchoring fibres (e.g. Sharpey's fibres), with which they could have a superficial resemblance. There is little doubt that they indeed represent a complex network of canaliculi, but with ramifications mainly developing at some distance from osteocyte bodies. This situation could indeed explain why it is difficult to clearly show that they originate from the osteocyte lacunae.

Vascular canals are mostly represented by primary osteons, whose lumen varies from 10 to 40 µm in diameter, depending on the level of the section, and the individual or species considered (Figs 3H, 4–6). Simple vascular canals are also observable, although they are less frequent and always associated, when present, to primary osteons. In many individuals of diverse taxa, the cortical layers (of periosteal origin) show a pronounced deflection under the vascular canals (Fig. 4B). This feature is evidence of the primarily periosteal origin of intra-cortical vascularization. Besides the primary osteons, some secondary osteons occur in the peri-medullary region of *Nanorana vicina* and *Pipa pipa* (Fig. 4A). Vascular canals have a preferential longitudinal orientation; however, oblique or even radial canals can be observed in association with longitudinal ones (Figs 3H, 4A, B, 5, 6). The distribution of the vascular canals, regardless of their nature, can be random (Fig. 4C), but this condition is rare; they rather tend to be organized either in radial rows (Figs 4D, 5B, 6A–D), or in circumferential layers (Fig. 4F), or in a combination of both. In *Rhinella marina*, the primary osteons are arranged in concentric layers and tend to have a circumferential orientation (Fig. 4F); this locally gives the bone an apparent laminar organization (but the latter does not correspond, of course, to a fibro-lamellar complex).

Statistical analyses

Basic statistical results

In Caudata, the occurrence of intra-cortical vascular canals in the 54 long bones of our sample has a frequency rate of 3.7%, and involves only the two *Andrias* species [albeit with extremely low *VD* values (0.09 to 0.18) and only in the femur; the humerus being completely avascular]. Among the 62 bones of our anuran sample, 20 display vascular canals, that is, 32.3% (Appendix). Basic statistics of the data suggest that the occurrence of vascular canals is more frequent in the humerus (40.7%) than in the femur (26.5%) of anurans. However, a binomial test on the number of evolutionarily independent appearances of vascular canals in the humerus (3) and the femur (5) indicates that there is no significant pattern here ($P = 0.7266$ for having a distribution at least that asymmetrical). This test was performed on our entire batrachian sample to increase its power a little. Similarly, Fisher's exact test (a non-phylogenetic test, also performed on the whole batrachian sample, but on the frequency of the occurrence of vascularization in both clades) again fails to find a statistically significant difference ($P = 0.4798$). The average VD (10.97 ± 17.91 for the humerus and 9.61 ± 19.67 for the femur) is not significantly different between these bones (Mann–Whitney: $P = 0.3878$).

Phylogeny-informed analyses

Basic statistics and visual inspection of the data suggest that anurans are more frequently vascularized than urodeles; however, a phylogenetic binomial test (Smith *et al.*, 2013) fails to find statistical support for this pattern ($P = 0.2090$ for the femur and 0.1136 for the humerus). Similarly, continuous analysis failed to detect a significant shift in VD between both clades for the femur and the humerus because the 78% confidence intervals of their base nodes overlap broadly. This is not surprising given that we failed to find a phylogenetic signal in this character (VD), for both bones (see below). However, these results need to be interpreted cautiously because VD, even after logarithmic transformations, shows strong departure from Brownian motion, so this, combined with the apparent absence of a phylogenetic signal suggests that the character optimizations on which this test is based are not necessarily reliable.

About a third of the characters show a phylogenetic signal (Table 2). This concerns the total cross-section area (A_{tot}), average CT and maximal diameter (MD) of both bones, as well as the PLg and the mass-specific resting metabolic rate (ln-transformed MR) of the taxa.

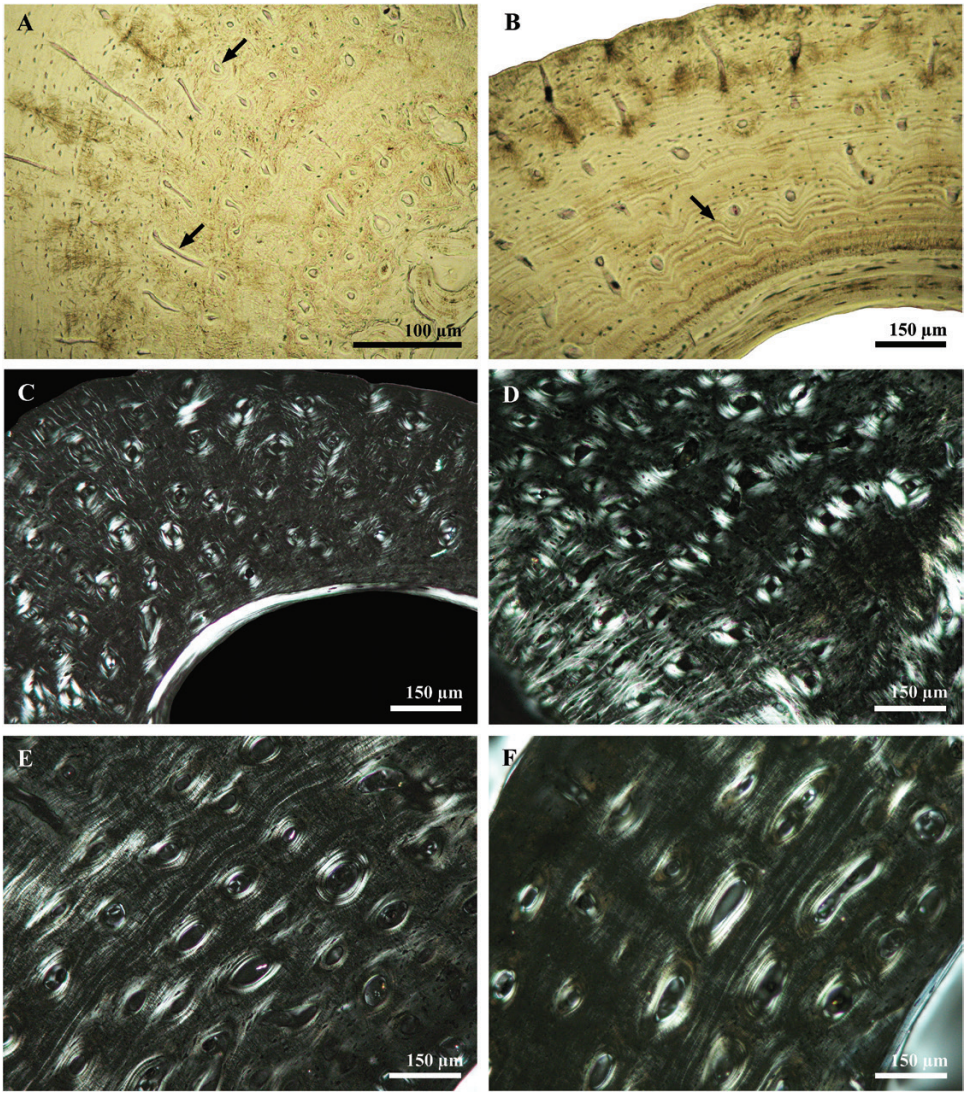

Figure 4. Vascular canals in the bones of anurans. (A) Variably oriented canals (radial, oblique, longitudinal) in the humeral cortex of *Pipa pipa* (individual N° 1 of specimen MNHN.AC.1954.325). The arrows point to a radial canal and a primary osteon; (B) Deflection of cortical bone layers (arrow) under vascular canals in the humeral cortex of *P. pipa*; (C) longitudinally oriented primary osteons, with a random spatial distribution, in the femoral cortex of *Amietophrynus regularis* (specimen MNHN. H. 163.63; polarized transmitted light); (D) longitudinal primary osteons forming radial rows in the femur of *A. regularis* (polarized transmitted light); (E) longitudinal primary osteons forming circular rows in the femur of *Rhinella marina* (specimen MNHN. AC. 1885-37; polarized transmitted light); (F) primary osteons with an incipient circumferential orientation forming concentric rows in the femur of *R. marina* (polarized transmitted light).

Most characters appear to have evolved according to a non-Brownian model, given that contrasts were adequately standardized in only three characters (out of 25; Table 3); logarithmic transformation of the data as well as branch length transformations did not help.

The FDR analysis indicates that for the 243 statistical tests that we performed, the corrected adjusted threshold to account for multiple tests is 0.02 (instead of the uncorrected 0.05 threshold). This allows us to filter 25 false positives, most of which concern artefact checks (to verify whether the characters evolved according to a Brownian motion model).

Three non-phylogenetic linear regressions between the VD (our dependent variable) and the three independent variables A_{tot}, RA_{cx} and CT (Fig. 7) fail to show a significant effect of these variables on vascular density. However, phylogenetic pairwise comparisons on the same data (Table 4) yield a significant effect of CT on VD for the femur (P = 0.0078), but not for the humerus (P = 0.0352; not significant according to

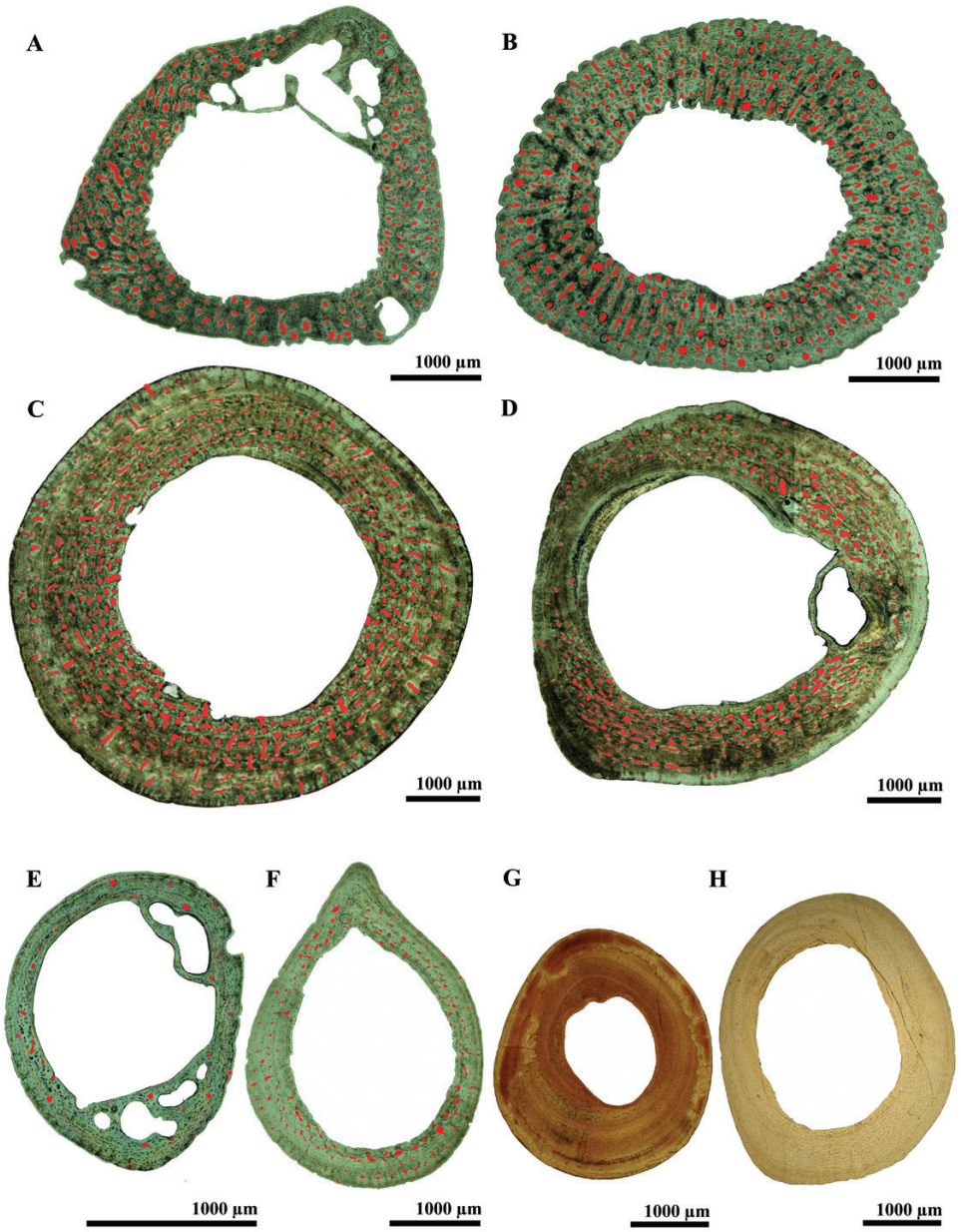

Figure 5. Mid-diaphyseal cross-sections of the humerus and femur of different-sized anuran species. The vascular canals have been highlighted in red. (A) *Lithobates catesbeianus* humerus (specimen L 2003-20); (B) *L. catesbeianus* femur (specimen L 2003-20); (C) *Rhinella marina* humerus (specimen MNHN. AC. 1885-37); (D) *R. marina* femur (specimen MNHN. AC. 1885-37); (E) *Sclerophrys pentoni* humerus (specimen L 2003-21); (F) *Ceratophrys aurita* femur (Specimen L 2003-5); (G) *Latonia gigantea* femur (specimen MNHN/PAL Sa 23480 B); (H) *L. gigantea* femur (Specimen MNHN/PAL Sa 23480 A).

FDR analysis). The total area of these bones (A_{tot}) does not appear to have a significant influence (P = 0.0625 and 0.1445, respectively). The influence of CT of the femur remains significant if these tests are performed on the batrachian (global) sample (P = 0.0047), though not on the humerus (P = 0.098), as expected. This effect is apparently not simply a threshold effect between thin-walled, avascular bones and larger, vascularized bones because repeating these tests by replacing VD (a quantitative character) by vascularization presence (a binary character) results in systematically higher probabilities, none of which is significant (Table 4).

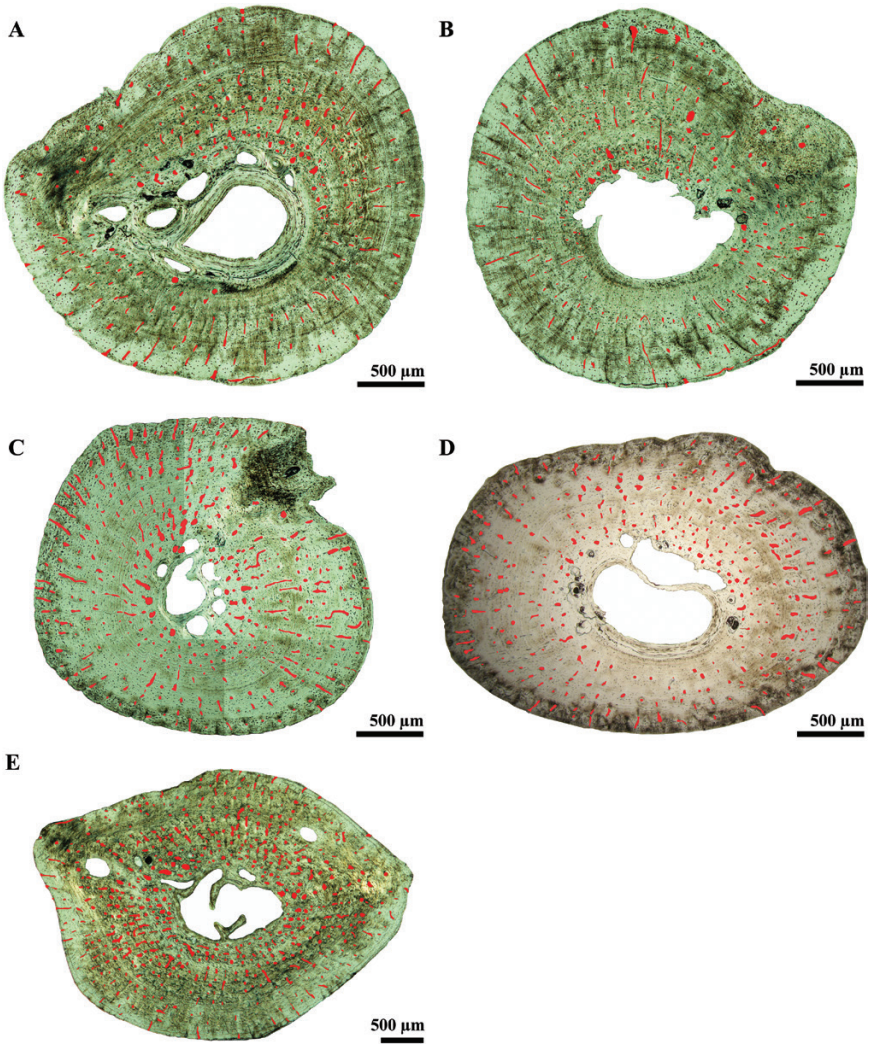

Figure 6. Mid-diaphyseal cross-sections of the humerus and femur of *Pipa pipa* showing the variability in microanatomical and vascularization patterns within a given bone (A–C), between two individuals (A–C vs. D) and between humerus (A–D) and femur (E). The vascular canals have been highlighted in red. (A) Humerus (specimen N° 1, section 1); (B) Humerus (Specimen N° 1, section 2); (C) Humerus (specimen N° 1, section 3); (D) Humerus (specimen N° 2); (E) Femur (specimen N° 1). All specimens come from a single jar that bears the number MNHN.AC.1954.325.

DISCUSSION

VASCULARIZATION PATTERNS

When present, bone vascularization of lissamphibians, mostly comprising simple vascular canals or primary osteons (as previously mentioned in Enlow & Brown, 1956; Ricqlès, 1976; Castanet *et al.*, 2003; Laurin, Canoville & Quilhac *et al.*, 2009) with various topographic arrangements, is morphologically similar to that of sauropsids (as described in Buffrénil *et al.*, 2008; Cubo *et al.*, 2014) and some marsupial mammals (e.g. Kolb *et al.*, 2015b). However, a nearly circumferential organization of the canals, as observed in *R. marina*, is unknown in extant lepidosaurs. Furthermore, the plexiform, reticular or true laminar organizations of the canals that prevail in eutherian mammals (Kolb *et al.*, 2015a, b), extant birds and most Mesozoic dinosaurs (Chinsamy-Turan, 2005; Legendre *et al.*, 2014), are absent in lissamphibians (as well as in extant lepidosaurs). Two groups of extinct limbed vertebrates, the lepospondyls and the temnospondyls, have been alternatively proposed as the closest relatives of Lissamphibia (e.g. Anderson *et al.*, 2008; Marjanović & Laurin, 2013). While the limb bone histology of lepospondyls is virtually unknown, temnospondyl bone histology has been extensively studied (e.g. Enlow & Brown, 1956; Ricqlès, 1975; Steyer *et al.*, 2004; Mukherjee *et al.*, 2010; Sanchez *et al.*, 2010a, b; Konietzko-Meier & Klein, 2013; Konietzko-Meier & Sander, 2013; Sanchez & Schoch, 2013; Canoville &

Table 2. Phylogenetic signal in the size and vascularization data

Characters	*P* values
Continuous characters – femur	
VA/A_{cx}	0.9282
VD (vc/mm^2)	0.7211
A_{tot} (mm^2)	**0.0034**
RA_{cx} (%)	0.0999
CT (mm)	**0.0133**
vc mean diameter (µm)	0.8524
MD (mm)	**0.0071**
Discrete characters – femur	
vc type	0.6142
vc orientation	0.7946
avascular (0); vascularized (1)	0.8719
Continuous characters – humerus	
VA/A_{cx}	0.9117
VD (vc/mm^2)	0.6323
A_{tot} (mm^2)	**0.0011**
RA_{cx} (%)	0.6167
CT (mm)	**0.0012**
vc mean diameter (µm)	0.6571
MD (mm)	**0.0109**
Discrete characters – humerus	
vc type	0.3235
vc orientation	0.8225
avascular (0); vascularized (1)	0.9181
Continuous characters – taxa	
PLg (cm)	**0.0048**
MR (ml O_2 g^{-1} h^{-1}) 15 °C. ln transformed	**0.0083**
Body mass (g) 15 °C	0.1437
MR (ml O_2 g^{-1} h^{-1}) 20 °C	0.4747
Body mass (g) 20 °C	0.5500

Significant results (after correction for multiple tests) are in bold type. A_{tot}, total area of the cross-section; CT, absolute cortical thickness; MD, maximal diameter of the cross-section; MR, mass-specific resting metabolic rate; PLg, presacral length; RA_{cx}, relative area of the cortex; VA, area of vascular canals; vc, vascular canals; VD, vascular density.

Chinsamy, 2015). In general, small temnospondyls tend to have very simple bone structures, with poorly vascularized to avascular cortices (Sanchez *et al.*, 2010b), similar to extant urodeles and some, usually small, anurans (Skutschas & Stein, 2015). Larger forms exhibit much more variable and complex vascularization patterns, in some cases with highly vascularized incipient-fibrolamellar bone tissues unknown from extant lissamphibians and lepidosaurs (Castanet *et al.*, 2003; Konietzko-Meier & Klein, 2013; Konietzko-Meier & Sander, 2013; Skutschas & Stein, 2015).

A comparative review of published data reveals that, although the vascular network in lissamphibians is generally much less dense than that of birds [e.g. VD = 149.6 vc/mm^2 in *Bubulcus ibis* (maximal length = 560 mm; Scott, 1987); Cubo *et al.*, 2014], it, nonetheless, has an upper limit [VD = 63 vc/mm^2 in *Amietophrynus regularis* (SVL = 130 mm; Rödel, 2000)] higher than that reported for lepidosaurs [VD = 43.8 vc/mm^2 in *Varanus rudicollis* (SVL = 590 mm; Harrison & Lim, 1957); Cubo *et al.*, 2014). This conclusion is based on data from 13 anuran species in our sample that display vascularization in the humerus or the femur, four of which display a VD > 43.8 vc/mm^2.

Finally, the existence of a potential size threshold separating avascular bones from vascularized ones, had been previously suggested by Castanet *et al.* (2003) for anurans, and complies with a general pattern already described in amniotes by Buffrénil *et al.* (2008) and Cubo *et al.* (2014). Unfortunately, the disparity of the data available in the literature hampers precise comparison of the thresholds.

Phylogenetic signal

The results of this study suggest that VD is not significantly influenced by phylogeny in Lissamphibians. Previous works by Cubo *et al.* (2005) and Legendre *et al.* (2012, 2014) reached the opposite conclusion in amniotes; phylogeny explains a great percentage of the variance of vascular density, irrespective of the statistical methods used. Our results suggest that several parameters more or less directly related to the specific size of taxa (A_{tot}, MD and CT) are sensitive to phylogenetic relationships and, at least in the case of femoral CT, can have an influence on vascular density. In the latter case, phylogeny would thus rank as a secondary, or indirect, explanatory factor for vascular density. Recent studies in diapsids in general (Cubo *et al.*, 2014) and varanids in particular (Buffrénil *et al.*, 2008) reached a similar conclusion.

Differences between urodeles and anurans

At a gross micro-anatomical level, a striking difference between urodeles and anurans is the irregular, patchy resorption occurring in the core of bone cortices in some urodeles. This feature mentioned or illustrated by Ricqlès (1964), Castanet *et al.* (2003) and Buffrénil *et al.* (2015) seems to be unknown in anurans and other tetrapods. Up to now, its developmental pattern and functional involvements remain poorly documented; future studies should specifically address this intriguing question.

Among the 21 genera of urodeles studied, only one, *Andrias*, displays vascularized cortices in stylopodial bones. Considering that the femur of *A. davidianus* is slightly smaller than that of *A. japonicus*, it is possible that its size (A_{tot} = 20.3 mm^2) is close to the threshold beyond which vascularization appears in the urodele long bones. However, this interpretation would only be valid for the femur, because the humerus of

Table 3. Artefacts standardization of the FIC, showing non-Brownian evolution in the characters

Characters	*P* test 1	2	3	4	Standardized 0, no; 1, yes
Continuous characters – femur	0.0186	4.72E–13	0.0297	0.0101	0
VA/A_{cx}	0.0272	4.13E–08	0.0131	0.01	0
VD (vc/mm^2)	0.4693	1.50E–08	0.3716	0.5318	0
A_{tot} (mm^2)	6.25E-04	5.92E–02	0.0143	0.0102	0
RA_{cx}	0.089	5.71E–07	0.1977	0.5308	0
CT (mm)	0.0186	4.72E–13	0.0297	0.0101	0
vc mean diameter (µm)	0.0152	8.42E–14	0.1082	0.0848	0
MD (mm)	0.1016	3.31E–05	0.1254	0.8034	0
Discrete characters – femur					
vc type	0.0782	1.71E–05	0.0155	0.0105	0
vc orientation	0.0235	2.41E–08	0.0157	0.0159	0
avascular (0); vascularized (1)	0.1646	1.04E–07	0.1853	0.9963	0
Continuous characters – humerus					
VA/A_{cx}	0.0031	4.29E–12	0.0135	0.0098	0
VD (vc/mm^2)	0.0118	2.54E–05	0.0342	0.0164	0
A_{tot} (mm^2)	0.4368	1.29E–06	0.3617	0.9197	0
RA_{cx}	0.178	3.10E–03	0.497	0.009	0
CT (mm)	0.2756	2.69E–07	0.5138	0.6892	0
vc mean diameter (µm)	0.0122	1.30E–03	0.036	0.0053	0
MD (mm)	0.2041	1.73E–05	0.0621	0.0788	0
Discrete characters – Humerus					
vc type	0.0587	9.10E–03	0.0902	0.0128	0
vc orientation	0.031	3.02E–04	0.0753	0.0137	0
avascular (0); vascularized (1)	0.0072	1.62E–01	0.1024	0.0142	0
Continuous characters – taxa					
PLg (cm)	0.4215	1.16E–10	0.1576	0.0469	0
MR (ml O_2 g^{-1} h^{-1}) 15 °C. ln-transformed	0.1623	1.66E–01	0.1858	0.8799	1
Body mass 15 °C	0.1816	8.20E–04	0.1357	0.011	0
MR (ml O_2 g^{-1} h^{-1}) 20 °C	0.7876	8.49E–02	0.3677	0.7789	1
Body mass 20 °C	0.8761	9.64E–02	0.9923	0.0448	1

The four documented tests concern linear regressions between: (1) absolute value of contrasts vs. their expected standard deviation (computed from branch lengths); (2) absolute value of contrasts vs. estimated node value; (3) absolute value of contrasts vs. node height (above root); (4) estimated node value vs. node height. All tests were performed by the PDAP module (Midford, Garland & Maddison, 2010) for Mesquite (Maddison & Maddison, 2014). A_{tot}, total area of the cross-section; CT, absolute cortical thickness; MD, maximal diameter of the cross-section; MR, metabolic rate; PLg, presacral length; RA_{cx}, relative area of the cortex; VA, area of vascular canals; vc, vascular canals; VD, vascular density.

A. japonicus, though larger (A_{tot} = 22.1 mm^2), is avascular. Among the extant urodeles sampled in this study, the presence of vascular canals in limb bones is a peculiarity of *Andrias*, and no larger species exists in extant faunas. The presence of ridges terminated by foramina (most likely vascular) on the surface of long bones in *Ukrainurus hypsognathus* (from the Miocene of Ukraine; Vasilyan *et al.*, 2013) and *Aviturus exsecratus* (from the Paleocene–Eocene of Mongolia; Vasilyan & Böhme, 2012), that are the only known urodeles larger than *Andrias* spp. (femoral diameter at mid-diaphysis is 8.08 and more than 10 mm, respectively, in these species, vs. 6.3 mm in our *A. japonicus* specimen), supports the hypothesis of such a threshold. A histological investigation of *Ukrainurus* and *Aviturus* bones could ascertain the nature of these foramina.

In previous studies, a few simple vascular canals have been reported in the long bone shafts of several salamander species, such as *Ambystoma tigrinum* (Enlow & Brown, 1956), as well as *Calitriton asper*, *P. waltl*, *Salamandra salamandra*, *S. atra Notophthalmus viridescens*, *Triturus cristatus* (Castanet *et al.*, 2003), *Ambystoma opacum*, *Salamandrella keyserlingii* and *Desmognathus monticola* (Laurin *et al.*, 2009). The last eight species have also been sampled in the present study, but our specimens did not have any vascular canals (Appendix). A check of the illustrations (when available) in previous original articles or sections suggests that the canals mentioned by these authors actually corresponded to initial nutrient canals (housing the nutrient artery), a kind of canal that we excluded from our computations (see above:

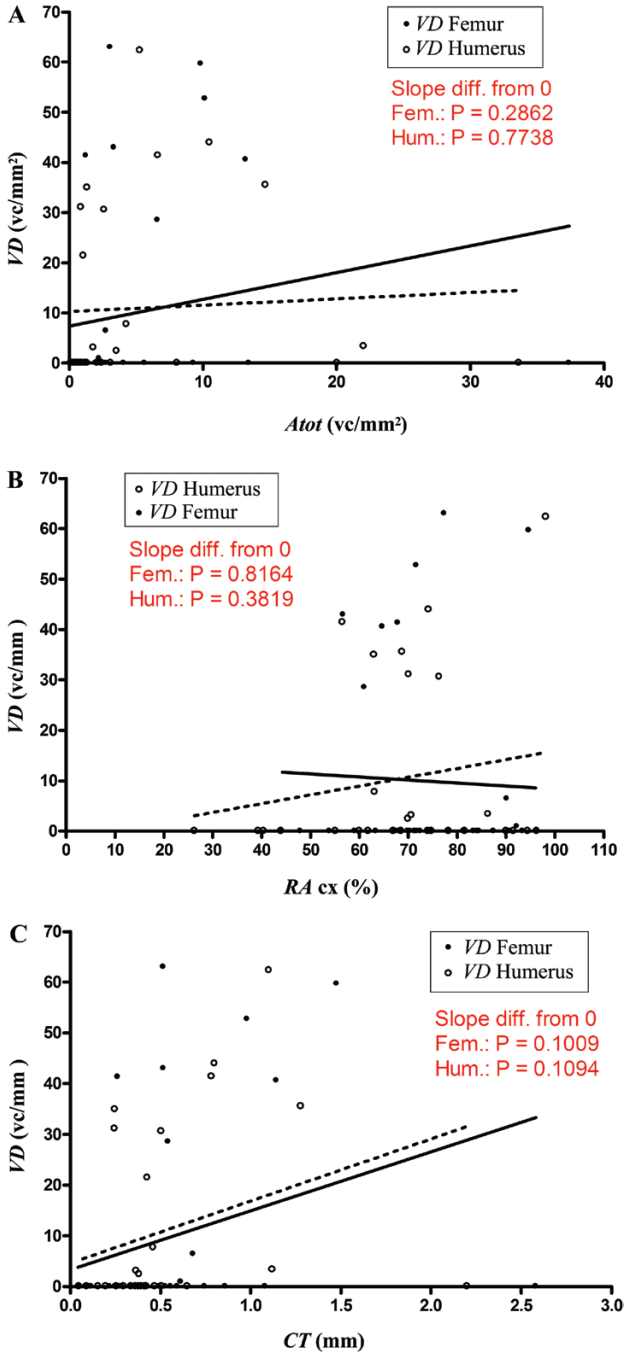

Figure 7. Linear regressions showing the relationships between the dependent variable VD and three independent morphometric variables: (A) total cross-section area (A_{tot}); (B) relative cortical area (RA_{cx}, in mm²); (C) absolute cortical thickness (CT, in mm). None of these three regressions reveals a significant relationship.

Material and Methods). If we limit the comparative analysis to extant forms, we can thus conclude that the presence of vascular canals in urodele limb bones is extremely rare. To date, the stylopod histology of only three Middle Jurassic stem-salamander taxa has been described (Buffrénil *et al.*, 2015; Skutschas & Stein, 2015). No clear vascular canals were observed in the humeral shafts of juvenile to subadult specimens of *Marmorerpeton* or Salamander A (Buffrénil *et al.*, 2015). Although small specimens (probably juveniles) of *Kokartus honorarius* have avascular cortices, larger ones (probably subadult to adult individuals) exhibit a few isolated longitudinal vascular canals, as well as secondary osteons in the proximal and distal shafts of their stylopods (Skutschas & Stein, 2015). Again, these differences in the presence of vascular canals in these stem-salamanders could be linked to a size threshold.

In anurans, bone vascularization is more common. However, none of the six humeri smaller than A_{tot} = 0.9 mm² (i.e. 21.4% of the humeri sampled) show vascularization. Likewise, none of the 11 femora smaller than A_{tot} = 1.2 mm² (32.4% of the femora) are vascularized. As for urodeles, it is thus possible that these size values correspond approximately to thresholds, below which anuran long bones remain avascular. Beyond these potential thresholds, only some of the bones show intra-cortical vascularization. Indeed, the bones of the medium-sized species *Latonia gigantea* (A_{tot} = 5.6 mm² for the femur, Appendix) are completely avascular (Fig. 5G, H), while for example, the femur of *Ceratophrys aurita* (A_{tot} = 3.3 mm², Appendix) is well-vascularized (Fig. 5F).

Our results thus show that the differences between urodeles and anurans do not only concern the vascular canal density, but also the threshold beyond which vascular canals appear (whatever the morphological character considered: A_{tot}, CT, etc.). These differences suggest that, although the statistical tests failed to show a significant difference between urodeles and anurans (probably due to a lack of power of our tests, resulting from the low number of species for which data on mass-specific metabolic rate exist), the process of bone vascularization is different in both groups.

Differences within anurans

When bone vascularization is present in anurans, it often shows relatively high values (71% of VD values are above 20 vc/mm², and 62% above 30 vc/mm²; Appendix); conversely some specimens have low VD values (0.96 vc/mm² for the *Nanorana* femur) and 67 % of all anuran bones sampled are avascular (Appendix). The cause of such differences in VD in anurans remains puzzling. There is a dual pattern in this taxon: (1) the existence of a size threshold below which vascularization is absent; (2) the increase in VD with the increase of cortical thickness. These results are congruent with previous observations that medium-sized and large anurans (that have, in general, thicker cortices)

Table 4. Relationship between bone size and vascularization

Independent character =>	A_{tot}			CT		
Dependent character	*P* values (Humerus)	*P* values (Femur)	Sign	*P* values (Humerus)	*P* values (Femur)	Sign
VD (all taxa)	0.196484	**0.035156**	+	0.098047	**0.004688***	**+**
VD (Anura)	0.144531	**0.0625**	+	0.035156	**0.007813***	**+**
Presence of vascularization (all taxa)	0.125	**0.078125**	+	0.125	**0.078125**	**+**
Presence of vascularization (Anura)	0.125	**0.1375**	+	0.125	**0.1375**	+

Pairwise comparisons, which are phylogeny-informed tests, were used here. Significant results are in bold type; those that remain significant after correction for multiple tests are marked with an asterisk. The sign of the relationship is indicated only when it is statistically significant (before correction for multiple tests).
A_{tot}, total area of the cross-section; CT, absolute cortical thickness; VD, vascular density.

tend to be vascularized, whereas smaller forms have avascular limb bones (Foote, 1916; Enlow & Brown, 1956; Castanet *et al.*, 2003; Laurin *et al.*, 2009). Also, for a given species, different sized-individuals can show variable bone vascular densities: according to Foote's observations (1916: plate 1), a young bullfrog (*Lithobates catesbeianus*) specimen exhibited avascular femoral cortices, while a larger and older specimen had well-vascularized and proportionally thicker bone walls. A third, medium-sized, individual showed intermediate states of CT and vascularization.

In our results, conflicting observations, such as the presence of a high VD in the femur of the medium-sized frog *P. pipa* and, to the contrary, the low VD (or complete lack of vascular canals) in larger species with thick cortices, such as *Trichobatrachus robustus* or *C. goliath*, suggest that the factors controlling the presence and development of bone vascularization are more complex than previously supposed, and remain insufficiently deciphered.

In diapsids, a simple relationship between VD and the specific size of taxa has been shown (Cubo *et al.*, 2014). This relationship was not verified in our lissamphibian sample (for PLg, though it was for cortical thickness). Nonetheless, a significant influence of CT seems to be a common pattern in lissamphibians and other tetrapods.

Comments on the possible influence of metabolism

Available data only partially support the hypothesis that VD could be directly influenced by basal metabolic rate in lissamphibians, and in tetrapods in general.

For lissamphibians, we found that urodele limb bones are generally less vascularized than those of anurans; this observation is congruent with the lower resting metabolic rate of urodeles (Gatten *et al.*, 1992; Chong & Mueller, 2013). However, resting metabolic rate, which is known to vary considerably in anurans (Taigen *et al.*, 1982) apparently only partly explains the variance of bone VD in this group. There is probably a dual (sometimes antagonistic) effect of absolute CT and resting metabolic rate on bone VD in anurans. Thus, some species with relatively high resting metabolic rates, such as *Pelophylax esculentus* or *Rana temporaria* [respective average MR (20 °C) = 0.1034 ml O_2 g^{-1} h^{-1} and MR (20 °C) = 0.1090 ml O_2 g^{-1} h^{-1}; cf. Gatten *et al.*, 1992; Appendix] have avascular femora with relatively thin-cortices (CT = 0.352 and 0.592 mm, respectively; Appendix), whereas *L. catesbeianus*, which has a lower metabolism [MR (20 °C) = 0.03955 ml O_2 g^{-1} h^{-1}; Gatten *et al.*, 1992; Appendix], possesses a highly vascularized femur with thicker cortices (VD = 53 vc/mm², CT = 0.98 mm; Appendix). The complex vascularization patterns observed in anurans could also be related to the incredibly diverse ecological adaptations found in this group (Duellman & Trueb, 1986). However, investigating the relationship between VD and lifestyle habits is beyond the scope of the present study.

Finally, when vascular canals are present in anurans, their density tends to be higher than in similar-sized lepidosaurs. However, several studies have shown that the general resting metabolism of anurans is approximately the same as that of similar sized lepidosaurs (Andrews & Pough 1985; Bennett & Dawson, 1976).

These observations, along with the scanty comparative elements available hitherto, suggest the importance of metabolism alone on bone VD should be reconsidered. They rather evoke, once again, a complex and still poorly understood situation. Therefore, inferences of metabolic rate based on VD have to be considered carefully, especially in extinct taxa, where VD must necessarily be compared with other histological features. Data currently available finally suggest that, among many putative parameters, the most universal ones to estimate growth rate, and thus indirectly metabolic rate, are: (1) the types of primary bone tissues (woven, parallel-fibred or lamellar) and (2) the

geometric organization of the vascular canals, that is, the radial, circumferential, plexiform or reticular patterns (Castanet *et al.*, 1996a, 2000a; Margerie *et al.*, 2002, 2004).

Conclusions and perspectives

Our results clearly show that one feature is correlated to the bone VD in lissamphibians: the absolute CT of the stylopod diaphysis. This result confirms the significance of geometric constraints on bone vascularization, as previously evoked by Cubo *et al.* (2014). The present study, nonetheless, shows the existence of very diverse, sometimes contradictory patterns, and highlights the complexity and multiplicity of factors likely to influence bone vascular density. Future works should investigate the processes underlying the inclusion of the periosteal vessels in the newly deposited osteoid. To date, there are very limited data available on this subject.

ACKNOWLEDGEMENTS

We are grateful to the numerous colleagues who accepted to give or facilitate access to extant or fossil bone samples for this study: Wolfgang Böhme (Zoological Research Museum Alexander Koenig, Bonn, Germany); Susan Evans (University College London, England); Francis Renoult and Daniel Robineau (Comparative Anatomy collections of the Museum National d'Histoire Naturelle, Paris, France); Hélène Francillon-Vieillot (University Paris 7, Paris, France); Anne-Marie Ohler (lissamphibian collections of the Museum National d'Histoire Naturelle, Paris, France); Jean-Claude Rage (Paleontological collections of the Museum National d'Histoire Naturelle, Paris, France); Victor Hugo Reynoso Rosales (Universidad Nacional Autonoma de México, Mexico). We also thank Filippo Bertozzo for helping dissecting some specimens at the Zoological Research Museum Alexander Koenig, Bonn, Germany. We thank the reviewers Pavel Skutschas and Alexandra Houssaye for their constructive comments and suggestions that improved our manuscript. We are also grateful to the editor, Louise Allcock, for her efficient handling of our submission.

REFERENCES

Abramoff MD, Magalhães PJ, Ram SJ. 2004. Image processing with ImageJ. *Biophotonics International* **11:** 36–42.

Amiet J-L. 2004. *Conraua goliath. The IUCN red list of threatened species 2004*: e.T5263A11121365. Available at: http://dx.doi.org/10.2305/IUCN.UK.2004.RLTS.T5263A11121365.en

Anderson JS, Reisz RR, Scott D, Fröbisch NB, Sumida SS. 2008. A stem batrachian from the early permian of texas and the origin of frogs and salamanders. *Nature* **453:** 515–518.

Andrews RM, Pough FH. 1985. Metabolism of squamate reptiles: allometric and ecological relationships. *Physiological Zoology* **58:** 214–231.

Ash AN, Bruce RC, Castanet J, Francillon-Vieillot H. 2003. Population parameters of *Plethodon metcalfi* on a 10-year-old clearcut and in nearby forests in the southern Blue Ridge Mountains. *Journal of Herpetology* **37:** 445–452.

Benjamini Y, Hochberg Y. 1995. Controlling the false discovery rate: a practical and powerful approach to multiple testing. *Journal of the Royal Statistical Society Series B (Methodological)* **57:** 289–300.

Bennett AF, Dawson W. 1976. Metabolism. In: Gans C, Dawson W, eds. *Biology of the Reptila, vol. 5. Physiology A*. London & New York: Academic Press, 127–223.

Buffrénil V de, Houssaye A, Böhme W. 2008. Bone vascular supply in monitor lizards (Squamata: Varanidae): influence of size, growth and phylogeny. *Journal of Morphology* **269:** 533–543.

Buffrénil V de, Canoville A, Evans SE, Laurin M. 2015. Histological study of karaurids, the oldest known (stem) urodeles. *Historical Biology* **27:**109–114.

Buffrénil V de, Clarac F, Canoville A, Laurin M. 2016. Comparative data on the differentiation and growth of bone ornamentation in gnathostomes (Chordata: Vertebrata). *Journal of Morphology* **277:** 634–670.

Brookes M. 1963. Cortical Vascularization and growth in foetal tubular bones. *Journal of Anatomy* **97:** 597–609.

Caetano MH, Castanet J, Francillon H. 1985. Détermination de l'âge de *Triturus marmoratus marmoratus* (Latreille 1800) du parc national de Peneda Gerês (Portugal) par squelettochronologie. *Amphibia-Reptilia* **6:** 117–132.

Caetano MH, Leclair R Jr. 1996. Growth and population structure of red-spotted newts (*Notophtalmus viridescens*) in permanent lakes of the Laurentian Shield, Quebec. *Copeia* **1996:** 866–874.

Caetano MH, Leclair R Jr. 1999. Comparative phenology and demography of *Triturus boscai* from Portugal. *Journal of Herpetology* **33:** 192–202.

Canoville A, Laurin M. 2009. Microanatomical diversity of the humerus and lifestyle in lissamphibians. *Acta Zoologica* **90:** 110–122.

Canoville A, Chinsamy A. 2015. Bone microstructure of the stereospondyl *Lydekkerina* huxleyi reveals adaptive strategies to the harsh post permian-extinction environment. *Anatomical Record* **298:** 1237–1254.

Castanet J, Grandin A, Abourachid A, de Ricqlès A. 1996a. Expression de la dynamique de croissance dans la structure de l'os périostique chez *Anas platyrhynchos*. *Comptes rendus de l'Academie des sciences. Serie III, Sciences de la vie* **319:** 301–308.

Castanet J, Francillon-Vieillot H, Bruce RC. 1996b. Age estimations in desmognathine salamanders assessed by skeletochronology. *Herpetologica* **52:** 160–171.

Castanet J, Rogers KC, Cubo J, Boisard JJ. 2000a. Periosteal bone growth rates in extant ratites (ostriche

and emu). Implications for assessing growth in dinosaurs. *Comptes rendus de l'Academie des sciences. Serie III, Sciences de la vie* **323:** 543–550.

Castanet J, Pinto S, Loth MM, Lamotte M. 2000b. Age individuel, longévité et dynamique de croissance osseuse chez un amphibien vivipare, *Nectophrynoides occidentalis* (Anoure, Bufonidae). *Annales de Sciences Naturelles* **21:** 11–17.

Castanet J, Francillon-Vieillot H, de Ricqles A, Zylberberg L. 2003. The skeletal histology of the Amphibia. In: Heatwole H, Davies M, eds. *Amphibian biology*, *Vol.* 5. Chipping Norton: Surrey Beatty, 1598–1683.

Chinsamy A, Elzanowski A. 2001. Evolution of growth pattern in birds. *Nature* **412:** 402–403.

Chinsamy-Turan A. 2005. *The microstructure of dinosaur bone: deciphering biology with fine-scale techniques*. Baltimore: The Johns Hopkins University Press.

Chong RA, Mueller RL. 2013. Low metabolic rates in salamanders are correlated with weak selective constraints on mitochondrial genes. *Evolution* **67:** 894–899.

Cubo J, Ponton F, Laurin M, de Margerie E de, Castanet J. 2005. Phylogenetic signal in bone microstructure of sauropsids. *Systematic Biology* **54:** 562–574.

Cubo J, Legendre P, de Ricqlès A, Montes L, de Margerie E, Castanet J, Desdevises Y. 2008. Phylogenetic, functional, and structural components of variation in bone growth rate of amniotes. *Evolution & Development* **10:** 217–227.

Cubo J, Le Roy N, Martinez-Maza C, Montes L. 2012. Paleohistological estimation of bone growth rate in extinct archosaurs. *Paleobiology* **38:** 335–349.

Cubo J, Baudin J, Legendre L, Quilhac A, Buffrénil V de. 2014. Geometric and metabolic constraints on bone vascular supply in diapsids. *Biological Journal of the Linnean Society* **112:** 668–677.

Duellman WE, Trueb L. 1986. *Biology of Amphibians*. New York: McGraw-Hill.

Enlow DH, Brown SO. 1956. A comparative histological study of fossil and recent bone tissues. Part I. *The Texas Journal of Science* **8:** 405–444.

Enlow DH, Brown SO. 1958. A comparative histological study of fossil and recent bone tissues. Part III. *The Texas Journal of Science* **10:** 187–230.

Evans SE, Milner AR. 1991. Middle Jurassic microvertebrate assemblages from the British Isles. In: Kielan-Jaworowska Z, Heintz N, Nakrem HA, eds. Fifth Symposium on Mesozoic Terrestrial Ecosystems and Biota. Oslo: Contributions from the Paleontological Museum, University of Oslo, 21–22.

Evans SE, Waldman M. 1996. Small reptiles and amphibians from the Middle Jurassic of Skye, Scotland. In: Morales M, ed. The Continental Jurassic. *Museum of Northern Arizona Bulletin* **60:** 219–226.

Faith DP. 1992. Conservation evaluation and phylogenetic diversity. *Biological Conservation* **61:**1–10.

Foote JS. 1911. The comparative histology of femoral bones. *Transactions of the American Microscopical Society* **30:** 87–140.

Foote JS. 1916. *A contribution to the comparative histology of the femur*. Smithsonian Contribution to Knowledge 35. Washington: Smithsonian Institution, 1916.

Francillon H. 1979. Etude expérimentale des marques de croissance sur les humerus et les fémurs de tritons crêtés (*Triturus cristatus cristatus* Laurenti) en relation avec la détermination de l'âge individuel. *Acta Zoologica (Stockholm)* **60:** 223–232.

Francillon H, Pascal M. 1985. Présences de lignes d'arrêt de croissance dans les os longs de *Pleurodeles poireti* Gervais. Leur éventuelle utilisation comme indicateur de l'âge individuel. *Bulletin de la Société Zoologique de France* **110:** 223–238.

Francillon H, Barbault R, Castanet J, Ricqlès A de. 1984. Etude complémentaire sur la biologie de l'amphibien desertícole *Bufo pentoni*: données de squelettochronologie et démographie. *Revue d'Écologie (Terre Vie)* **39:** 209–224.

Francillon-Vieillot H, Arntzen JW, Géraudie J. 1990a. Age, growth and longevity of sympatric *Triturus cristatus*, *T. marmoratus*, and their hybrids (Amphibia, Urodela): a skeletochronological comparison. *Journal of Herpetology* **24:** 13–22.

Francillon-Vieillot H, Buffrénil V de, Castanet J, Géraudie J, Meunier FJ, Sire J-Y, Zylberberg L, Ricqlès A de. 1990b. Microstructure and mineralization of vertebrate skeletal tissues. In: Carter JG, ed. *Skeletal biomineralization: patterns, processes and evolutionary trends*. New York: Van Nostrand Reinhold, 471–530.

Gatten RE Jr, Miller K, Full RJ. 1992. Energetics at rest and during locomotion. In: Fedder ME, Burggren W, eds. *Environmental physiology of the amphibians*. Chicago & London: University of Chicago Press, 314–377.

Germain D, Laurin M. 2009. Evolution of ossification sequences in salamanders and urodele origins assessed through event-pairing and new methods. *Evolution & Development* **11:** 170–190.

Hancox NM. 1972. *Biology of bone*. Cambridge: Cambridge University Press.

Houck LD, Francillon-Vieillot H. 1988. Tests for age and size effects on male mating success in a plethodontid salamander. *Amphibia-Reptilia* **9:** 135–144.

Harrison JL, Lim BL. 1957. Monitors of Malaya. *Malayan Nature Journal* **12:** 1–10.

Huttenlocker AK, Botha-Brink J. 2013. Body size and growth patterns in the therocephalian *Moschorhinus kitchingi* (Therapsida: Eutheriodontia) before and after the end-Permian extinction in South Africa. *Paleobiology* **39:** 253–277.

Huttenlocker AK, Botha-Brink J. 2014. Bone microstructure and the evolution of growth patterns in Permo-Triassic therocephalians (Amniota, Therapsida) of South Africa. *PeerJ* **2:** e325.

Josse S, Moreau T, Laurin M. 2006. *Stratigraphic tools for Mesquite*. Version 1.0. Available at: http://mesquiteproject.org/packages/stratigraphicTools/

Kolb C, Scheyer TM, Lister AM, Azorit C, de Vos J, Schlingemann MA, Rössner GE, Monaghan NT, Sánchez-Villagra MR. 2015a. Growth in fossil and extant deer and implications for body size and life history evolution. *BMC Evolutionary Biology* **15:** 19.

Kolb C, Scheyer TM, Veitschegger K, Forasiepi AM, Amson E, Van der Geer AA, Van den Hoek Ostende LW, Hayashi S, Sánchez-Villagra MR. 2015b. Mammalian

bone palaeohistology: a survey and new data with emphasis on island forms. *PeerJ* **3:** e1358.

Konietzko-Meier D, Klein N. 2013. Unique growth pattern of *Metoposaurus diagnosticus krasiejowensis* (Amphibia, Temnospondyli) from the Upper Triassic of Krasiejów, Poland. *Palaeogeography, Palaeoclimatology, Palaeoecology* **370:** 145–157.

Konietzko-Meier D, Sander PM. 2013. Long bone histology of *Metoposaurus diagnosticus* (Temnospondyli) from the Late Triassic of Krasiejów (Poland) and its paleobiological implications. *Journal of Vertebrate Paleontology* **33:** 1003–1018.

Lamm E-T. 2013. Preparation and sectioning of specimens. In: Padian K, Lamm ET, eds. *Bone histology of fossil tetrapods*. Berkeley: University of California Press, 55–160.

Laurin M. 2008. The splendid isolation of biological nomenclature. *Zoologica Scripta* **37:** 223–233.

Laurin M. 2004. The evolution of body size, Cope's rule and the origin of amniotes. *Systematic Biology* **53:** 594–622.

Laurin M, Canoville A, Quilhac A. 2009. Use of paleontological and molecular data in supertrees for comparative studies: the example of lissamphibian femoral microanatomy. *Journal of Anatomy* **215:** 110–123.

Laurin M, Canoville A, Germain D. 2011. Bone microanatomy and lifestyle: a descriptive approach. *Comptes Rendus Palevol* **10:** 381–402.

Legendre L, Le Roy N, Martinez-Maza C, Montes L, Laurin M, Cubo J. 2012. Phylogenetic signal in bone histology of amniotes revisited. *Zoologica Scripta* **42:** 44–53.

Legendre LJ, Segalen L, Cubo J. 2013. Evidence for high bone growth rate in *Euparkeria* obtained using a new paleohistological inference model for the humerus. *Journal of Vertebrate Paleontology* **33:** 1343–1350.

Legendre LJ, Bourdon E, Scofield RP, Tennyson AJ, Lamrous H, Ricqlès A, Cubo J. 2014. Bone histology, phylogeny, and palaeognathous birds (Aves: Palaeognathae). *Biological Journal of the Linnean Society* **112:** 688–700.

Legendre LJ, Guénard G, Botha-Brink J, Cubo J. 2016. Palaeohistological evidence for ancestral high metabolic rate in Archosaurs. *Systematic Biology* **65:** 989–996.

Liang G, Geng B, Zhao E. 2004. *Andrias davidianus. The IUCN Red List of Threatened Species 2004*: e.T1272A3375181. Available at: http://dx.doi.org/10.2305/IUCN.UK.2004.RLTS.T1272A3375181.en

Lima V, Arntzen JW, Ferrand NM. 2000. Age structure and growth pattern in two populations of the gloden-striped salamander *Chioglossa lusitanica* (Caudata, Salamandridae). *Amphibia-Reptilia* **22:** 55–68.

Maddison WP. 1991. Squared-change parsimony reconstructions of ancestral states for continuous-valued characters on a phylogenetic tree. *Systematic Biology* **40:** 304–314.

Maddison WP. 2000. Testing character correlation using pairwise comparisons on a phylogeny. *Journal of Theoretical Biology* **202:** 195–204.

Maddison WP, Maddison DR. 2014. *Mesquite: a modular system for evolutionary analysis*. Version 3. Available at: http://mesquiteproject.org

Maddison WP, FitzJohn RG. 2015. The unsolved challenge to phylogenetic correlation tests for categorical characters. *Systematic Biology* **64:** 127–136.

Margerie E de, Cubo J, Castanet J. 2002. Bone typology and growth rate: testing and quantifying 'Amprino's rule' in the mallard (*Anas platyrhynchos*). *Comptes Rendus Biologies* **325:** 221–230.

Margerie E de, Robin J-P, Verrier D, Cubo J, Groscolas R. 2004. Assessing the relationship between bone microstructure and growth rate: a fluorescent labeling study in the king penguin chick (*Aptenodytes patagonicus*). *Journal of Experimental Biology* **207:** 869–879.

Marjanović D, Laurin M. 2013. The origin(s) of extant amphibians: a review with emphasis on the "lepospondyl hypothesis". *Geodiversitas* **35:** 207–272.

Meslin C, Mugnier S, Callebaut I, Laurin M, Pascal G, Poupon A, Goudet G, Monget P. 2012. Evolution of genes involved in gamete interaction: evidence for positive selection, duplications and losses in vertebrates. *PloS one* **7:** e44548.

Miaud C. 1992. La squelettochronologie chez les *Triturus* (Amphibiens, Urodèles) à partir d'une étude de *T. alpestris*, *T. Helveticus* et *T. cristatus* du sud-est de la France. In: Baglinière JL, Castanet J, Conand F, Meunier FJ, eds. *Tissus durs et âge individuel des vertébrés*. Paris: ORSTOM; INRA, 363–384.

Midford P, Garland TJ, Maddison WP. 2010. PDAP Package for Mesquite. Version 1.16. Available at: http://mesquiteproject.org/pdap_mesquite/index.html

Misawa Y, Matsui M. 1999. Age determination by skeletochronology of the Japanese salamander *Hynobius kimurae* (Amphibia, Urodela). *Zoological Science* **16:** 845–851.

Montes L, Le Roy N, Perret M, Buffrénil V de, Castanet J, Cubo J. 2007. Relationship between bone growth rate, body mass and resting metabolism rate in growing amniotes: a phylogenetic approach. *Biological Journal of the Linnean Society* **92:** 63–76.

Montes L, Castanet J, Cubo J. 2010. Relationship between bone growth rate and bone tissue organization in amniotes: first test of Amprino's rule in a phylogenetic context. *Animal Biology* **60:** 25–41.

Morgan JD. 1959. Blood supply of growing rabbit's tibia. *The Journal of Bone and Joint Surgery* **41:** 185–203.

Mukherjee D, Ray S, Sengupta DP. 2010. Preliminary observations on the bone microstructure, growth patterns, and life habits of some Triassic temnospondyls from India. *Journal of Vertebrate Paleontology* **30:** 78–93.

Padian K, Stein K. 2013. Evolution of growth rates and their implications. In: Padian K, Lamm E-T, eds. *Bone histology of fossil tetrapods: advancing methods, analysis, and interpretation*. Berkeley and Los Angeles: University of California Press, 253–264.

Platz JE, Lathrop A. 1993. Body size and age assessment among advertising male chorus frogs. *Journal of Herpetology* **27:** 111–114.

Ricqlès A de. 1964. Formation des os longs des membres de *Pleurodeles waltii* (Michahelles). *Bulletin de la Société Zoologique de France* **34:** 797–808.

Ricqlès A de. 1965. Formation des os longs des membres de *Pleurodeles waltii* (Michahelles). Deuxième partie. *Bulletin de la Société Zoologique de France* **40:** 267–286.

Ricqlès A de. 1975. Recherches paléohistologiques sur les os longs des Tétrapodes: 7. Sur la classification, la signification fonctionnelle et l'histoire des tissus osseux des Tétrapodes. Première Partie. *Annales de Paléontologie (Vertébrés)* **61:** 51–129.

Ricqlès A de. 1976. Recherches paléohistologiques sur les os longs des Tétrapodes: VII. Sur la classification, la signification fonctionnelle et l'histoire des tissus osseux des Tétrapodes. Deuxième partie. Fonctions: considérations fonctionnelles et physiologiques. *Annales de Paléontologie (Vertébrés)* **62:** 71–126.

Rödel MO. 2000. *Herpetofauna of West Africa, Vol. I. Amphibians of the West African Savanna*. Frankfurt: Edition Chimaira.

Sanchez S, Germain D, De Ricqlès A de, Abourachid A, Goussard F, Tafforeau P. 2010a. Limb-bone histology of temnospondyls: implications for understanding the diversification of palaeoecologies and patterns of locomotion of Permo-Triassic tetrapods. *Journal of Evolutionary Biology* **23:** 2076–2090.

Sanchez S, Steyer JS, Schoch RR, Ricqlès A de. 2010b. Palaeoecological and palaeoenvironmental influences revealed by long-bone palaeohistology: the example of the Permian branchiosaurid *Apateon*. *Geological Society, London, Special Publications* **339:** 139–149.

Sanchez S, Schoch RR. 2013. Bone histology reveals a high environmental and metabolic plasticity as a successful evolutionary strategy in a long-lived homeostatic triassic temnospondyl. *Evolutionary Biology* **40:** 627–647.

Scott SL. 1987. *Field guide to the birds of North America*. Washington: National Geographic Society, 464.

Skutschas P, Stein K. 2015. Long bone histology of the stem salamander *Kokartus honorarius* (Amphibia: Caudata) from the Middle Jurassic of Kyrgyzstan. *Journal of Anatomy* **226:** 334–347.

Smirina EM. 1994. Age determination and longevity in amphibians. *Gerontology* **40:** 133–146.

Smirina EM, Roček Z. 1976. On the possibility of using annual bone layers of alpine newts, *Triturus alpestris* (Amphibia: Urodela), for their age determination. *Věstnik Československé Společnosti Zoologické* **40:** 232–237.

Smirina EM, Serbinova IA, Makarov AN. 1994. Some complicated cases of age determination using the annual layers of bone in amphibians (at the example of the long-tailed salamander *Onychodactylus fisheri* (Amphibia, Hynobiidae). *Zoological Journal (Moscow)* **73:** 72–81.

Smith HF, Parker WH, Kotzé SH, Laurin M. 2013. Multiple independent appearances of the cecal appendix in mammalian evolution and an investigation of related ecological and anatomical factors. *Comptes Rendus Palevol* **12:** 339–354.

Steyer JS, Laurin M, Castanet J, Ricqlès A de. 2004. First histological and skeletochronological data on temnospondyl growth: palaeoecological and palaeoclimatological implications. *Palaeogeography, Palaeoclimatology, Palaeoecology* **206:** 193–201.

Taigen TL, Emerson SB, Pough FH. 1982. Ecological correlates of anuran exercise physiology. *Oecologia* **52:** 49–56.

Trias A, Fery A. 1979. Cortical circulation of long bones. *The Journal of Bone and Joint Surgery* **61:** 1052–1059.

Vasilyan D, Böhme M. 2012. Pronounced peramorphosis in lissamphibians–Aviturus exsecratus (Urodela, Cryptobranchidae) from the Paleocene-Eocene Thermal Maximum of Mongolia. *PLoS ONE* **7:** e40665.

Vasilyan D, Böhme M, Chkhikvadze VM, Semenov YA, Joyce WG. 2013. A new giant salamander (Urodela, Pancryptobrancha) from the Miocene of eastern Europe (Grytsiv, Ukraine). *Journal of Vertebrate Paleontology* **33:** 301–318.

Verrell PA, Francillon H. 1986. Body size, age and reproduction in the smooth newt, *Triturus vulgaris*. *Journal of Zoology London (A)* **210:** 89–100.

Wake DB, Castanet J. 1995. A skeletochronological study of growth and age in relation to adult size in *Batrachoseps attenuatus*. *Journal of Herpetology* **29:** 60–65.

SUPPORTING INFORMATION

Additional Supporting Information may be found in the online version of this article at the publisher's web-site:

Appendix. Complete data set. Abbreviations: I Os., primary osteons; II Os., secondary osteons; A_{tot}, total area of the cross-section; CT, absolute cortical thickness; L, longitudinal; MD, maximal diameter; MR, mass-specific metabolic rate; Obl., oblique; PLg, presacral length; $RA_{cx,}$ relative area of the cortex expressed in percent of the A_{tot}; RA_{vc}, relative area occupied by vascular canals; SVC, simple vascular canals; vc D, vascular canal diameter; VD, vascular density.